Incremental Sliding Mode Control for Aeroelastic Launch Vehicles with Propellant Slosh

Mooij, E.; Wang, Xuerui

DOI
10.2514/6.2021-1221

Publication date
2021

Document Version
Final published version

Published in
AIAA Scitech 2021 Forum

AIAA SciTech Forum
11–15 & 19–21 January 2021, VIRTUAL EVENT
AIAA Scitech 2021 Forum

10.2514/6.2021-1221

Check for updates

Incremental Sliding Mode Control for Aeroelastic Launch Vehicles with Propellant Slosh

Erwin Mooij* and Xuerui Wang†

Delft University of Technology, Faculty of Aerospace Engineering,

Kluyverweg 1, 2629 HS Delft, The Netherlands

This paper focuses on the attitude control and propellant slosh suppression of aeroelastic launch vehicles. Four candidate controllers are proposed: the Linear Quadratic Regulator (LQR), the Incremental Non-linear Dynamic Inversion (INDI) control, the Incremental Sliding Mode Control (INDI-SMC), and the Feedback Linearisation-based Sliding Mode Control (FL-SMC). Theoretical analyses show INDI itself is unable to deal with under-actuated systems. Therefore, when applied to the launch vehicle directly, it cannot simultaneously track the pitch command and effectively suppress the slosh dynamics. This issue is solved by INDI-SMC, which also has enhanced robustness against both matched and unmatched uncertainties. Furthermore, despite its reduced model dependency, INDI-SMC has better robustness against model uncertainties and external disturbances than FL-SMC. These merits of INDI-SMC are verified by various simulation results. First, when the nominal plant configuration is adopted, the system using INDI-SMC has the smallest pitch-angle tracking error. The slosh motion is also effectively damped out. Second, Monte-Carlo studies are used to test the robustness of LQR, INDI-SMC, and FL-SMC to parametric uncertainties. Among these three controllers, LQR shows the worst performance and largest control-effort outliers. On the contrary, both INDI-SMC and FL-SMC can resist a wider range of perturbations without significant performance degradation. Even so, the tracking and slosh damping performance of INDI-SMC is still the best. Finally, both INDI-SMC and FL-SMC show robustness against unmodeled dynamics, while the robust performance of INDI-SMC is superior.

I. Introduction

Long and slender bodies, such as (small) conventional launch systems, may suffer from an unwanted coupling between the rigid-body and flexible modes, which can lead to stability and controllability issues when not properly dealt with. This coupling may be amplified by the large variation of mass properties (due to oxidiser and fuel consumption), as well as the change in operational conditions, because of the large flight and altitude regime. The flexible modes can be excited by wind (gusts) and turbulence. An additional complication may arise for launchers with liquid-propellant propulsion systems, as (part of) the fuel and oxidiser may start moving in their corresponding tanks. These so-called sloshing effects can create a dynamic coupling with the rigid and/or flexible body that is not trivial to suppress. This is further complicated by the time-varying nature of the dynamic coupling, since the tank filling grades change significantly during the flight.

Stability of aeroelastic launchers has been studied for many years[1–3] and invariably focussed on the interaction between rigid and flexible modes, and the response to wind gust and turbulence, or the impact of aeroelasticity on control-system stability margins, *e.g.,* the work covered in Ref. 4. Part of our previous work focussed on the effect of aeroelasticity on launch-vehicle stability, controllability, and controller performance at a single point during the ascending flight,[5] as well as the additional effect of wind gust and turbulence during the trajectory from lift-off to burnout of the first stage, taking transient effects into account.[6]

*Associate Professor, Section Astrodynamics and Space Missions, e.mooij@tudelft.nl, Associate Fellow AIAA.
†Assistant Professor, Section of Aerospace Structures and Computational Mechanics & Section of Control and Simulations, x.wang-6@tudelft.nl, AIAA Member.

Many authors have studied the effect of sloshing on the stability and controllability of launchers and satellites.[7–11] Cui *et al.* discuss the parametric resonance of small-amplitude sloshing and show stability diagrams for different sloshing damping.[7] Non-linear slosh damping is also included in the stability analysis in Ref. 8 to come up with a relationship between the non-linear slosh damping and equivalent linear damping at a given slosh amplitude. Also, a more accurate (analytical) prediction of the danger zone of slosh mass locations is given when the launcher is controlled by proportional-derivative feedback. Using a multi-body formulation and bifurcation analysis, the neutral stability curves for a typical launcher in planar atmospheric flight are obtained in Ref. 9, and Bode plots are provided for the linearised system. In terms of control, the non-linear dynamics and control of a launcher's upper-stage are considered by applying Lyapunov-based non-linear feedback control laws with thrust-vector control.[10,11]

Most of the performed studies, especially when related to control-system design, assume perfect knowledge of the slosh motion, by applying an equivalent mechanical model. Stabilising the system with a simple PD controller and inspecting the gain and phase margins, shows that sloshing has a major effect and poses a problem for a standard proportional-derivative control system.[12,13] A significant and increasing control effort is in that case required to stabilise the vehicle, but when the slosh states (position and velocity of the slosh mass) are fed back, the performance improves significantly. However, when the slosh states are required in the feedback laws it is not necessarily true that this "perfect" knowledge is available. The motion of the liquid cannot directly be measured, and dedicated slosh "observers" may have to be developed to estimate the required slosh states.

In Ref. 13, a sliding-mode observer was designed to estimate the slosh states of the LOX and RP-1 tanks of the first stage of a rigid launch vehicle. The nominal performance of the observer, *i.e.,* when simulation and observer model are identical in terms of slosh parameters (mass, eigenfrequency, location, and damping factor), was shown to be excellent. The convergence of the observer error dynamics was achieved in at most 10 seconds, so only a short initialisation time was required before activating the control system. Small oscillations of the slosh masses persisted after a step response, with a frequency close to the natural frequency of the slosh masses. The PD controller could not remove these, and the swivel commands exhibited some form of limit-cycle behaviour.

A robustness analysis showed that when the slosh-observer parameters start deviating from the implemented slosh model, the performance is very sensitive to these differences. With only a two-percent variation, some outliers exhibited a doubling of the control effort and slosh motion. With a 5% variation, though, the (maximum) integrated slosh position had more than doubled, whereas the oscillatory behaviour had even tripled. Despite the fact that also in that case the rigid-body response was not so much affected, quite a large number of outliers pointed to a significant increase in control effort, as well as strong fluctuations in the control command. The combination with engine and flexible-body dynamics in the simulation model did lead to significant performance degradation of the observer.

The origin of this could be traced back to the poor performance of the PD controller, and a simple test with a rigid-body Incremental Non-linear Dynamic Inversion (INDI) controller increased robustness significantly. It did exhibit a form of limit-cycle behaviour, though, because feedback of the slosh states was lacking. Therefore, priority in this paper is given to the development of a more robust controller that includes the feedback of slosh signals.

To further enhance the robustness of INDI control, the Incremental Sliding Mode Control (INDI-SMC) framework was proposed.[19] This hybrid framework was derived for generic multi-input/multi-output non-linear uncertain systems. Lyapunov-based analyses and extensive simulation cases show that INDI-SMC is able to resist a wide range of model uncertainties, sudden actuator faults, and structural damage with reduced sliding mode control/observer gains. Real-world quadrotor flight tests also demonstrated the effectiveness and easy implementation of INDI-SMC.[20] Furthermore, INDI-SMC can achieve high-order sliding modes with finite-time convergence.[21] More importantly, as compared to the conventional model-based SMC designs in literature, the control model dependency and sliding mode control/observer gains are simultaneously reduced in the INDI-SMC framework.

This paper has two theoretical contributions as compared to the INDI-SMC designs in literature:[19,20] first, by exploiting the null space, the sliding surface designed in this paper ensures the robustness of the controller against *unmatched* uncertainties; second, this paper presents the design and Lyapunov-based stability proofs of INDI-SMC for *under-actuated* dynamic systems. Furthermore, the presented theories are validated by applying INDI-SMC to a command tracking problem of an aeroelastic launch vehicle with propellant slosh.

As a reference, the two-stage PacAstro launcher for small payloads up to 225 kg has been selected for continuity of the research and the availability of launcher data[a]. The launcher is treated as a flexible beam with lumped masses to account for the subsystems and the fuel.[5,6,13] Modelling of the slosh motion will be done for oxidiser and fuel separately, with one tank each per stage of the selected two-stage launcher.

The layout of this paper is as follows. Section II will discuss the simulation model, *i.e.,* the combination of the rigid system with coupled slosh dynamics. Some remarks will be made about the coupling with engine dynamics and flexible modes, although studying those coupling effects is not the main focus of this paper. These effects will be included as perturbations, once the controller has been properly designed. Section III presents the incremental sliding mode controller. For comparisons, the conventional sliding mode control based on feedback linearisation is also shown in Sec. III. Next, in Sec. IV, the results of the study are shown, split into two parts: first, the nominal case is considered, and second, parameter uncertainties in the slosh model are taken into account. Section V, finally, concludes this paper.

II. Flight-Dynamics Model

For stability and controllability studies of flexible launchers, it is common practise to focus on pitch-plane motion only, and then even considering a linearised system that represents the error dynamics. Following this approach, in previous work the state-space model for a flexible launcher with engine dynamics and coupled slosh dynamics has been derived.[5,12] In this section we will summarise this model, but refrain from the detailed mathematical expressions; the reader is referred to the earlier mentioned references.

The flexible-launcher configuration that serves as the basis for the state-space model describing the error dynamics is shown in Fig. 1. Input to this error-dynamics model is a modal description as a function of current mass, the normal-load and pitch-moment distribution, and, of course, the flight conditions. The launcher is assumed to move with a steady-state velocity u_0. Its rotational states are the pitch angle, θ, and its derivative the pitch rate, q, and the angle of attack, α, that originates from the vertical velocity and has been added to allow for adding wind effects as a perturbation in angle of attack. The local deformation is determined by the combination of thrust, T, gravity, mg_d, aerodynamic normal force, N, and aerodynamic pitch moment, M. The structural model is represented by a (discretised) flexible beam, and its modal shapes have been used to include the effects of elastic line deformation in the aerodynamic coefficients. Finally, the engine is assumed to be 100% throttleable, and its direction is given by the swivel angle, ε_T. The swivel is modelled as a third-order dynamics system.

The liquid motion in the fuel and oxidiser tanks will introduce perturbing accelerations that affect the motion of the launcher. Besides the actual slosh dynamics, sloshing will introduce coupling effects with the rigid translational and rotational motion, as well as with the flexible-body dynamics. In Fig. 2 the configuration of the flexible launcher is shown, with two slosh masses, $m_{s,1}$ and $m_{s,2}$, for the RP-1 and LOX tanks of the first stage, and two for the second stage ($m_{s,3}$ and $m_{s,4}$), albeit that in this paper it is assumed that the second-stage tanks do not experience any sloshing.

The slosh model for a cylindrical tank (partially) filled with fuel or oxidiser is based on a damped mass-spring system (see also Fig. 3). Abramson, in Refs. 15 and 16, as well as Dodge in Ref. 17, provide a simple model to calculate n_s eigenfrequencies for different tank shapes, including the cylindrical one. The model has been adapted for a partial filling grade, and damping of the (primary) slosh mode is based on the model derived from the experimental study by Stephens *et al.*[18] In summary, each slosh mode is defined by its mass, m_s, the location with respect to the launcher's centre of mass, ℓ_s, the spring stiffness, k_s, and damping constant, c_s.

In its general form, the system equation of the extended state-space model that is used for the plant (launcher) is given by

$$\mathbf{E}\dot{\mathbf{x}} = \mathbf{A}\mathbf{x} + \mathbf{B}\mathbf{u} \tag{1}$$

or

$$\dot{\mathbf{x}} = \mathbf{E}^{-1}\mathbf{A}\mathbf{x} + \mathbf{E}^{-1}\mathbf{B}\mathbf{u} = \mathbf{A}'\mathbf{x} + \mathbf{B}'\mathbf{u} \tag{2}$$

[a]PacAstro was a US transportation service company, formed in 1990, to provide low-cost transportation of small satellites to Low Earth Orbit for approximately \$5 million per launch using proven technology.[14] Unfortunately, the launcher never came to operation despite several engine tests and three launch contracts, due to the lack of development funding. The company ceased to be in 1997.

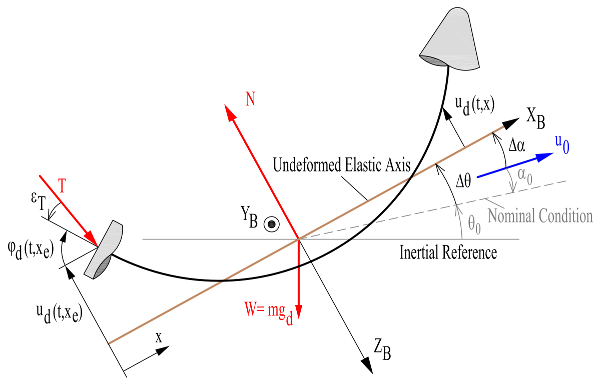

Figure 1. Flexible vehicle definitions

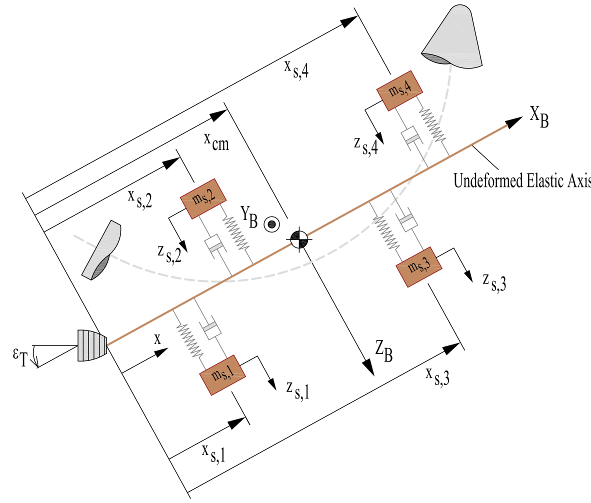

Figure 2. Slosh configuration of the flexible launcher

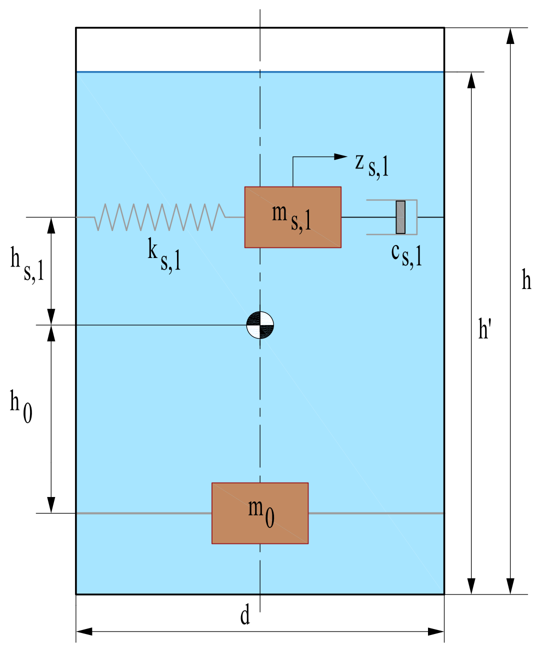

Figure 3. Slosh geometry for a cylindrical tank (single mode).

with the state and control vector given by $\mathbf{x}^{\mathrm{T}} = \left(\alpha\,\theta\,q\,\ddot{\varepsilon}_T\,\dot{\varepsilon}_T\,\varepsilon_T\,\dot{\eta}_1\,\eta_1 \ldots \dot{\eta}_{n_f}\,\eta_{n_f}\,\dot{z}_{s,1}\,z_{s,1} \ldots \dot{z}_{s,n_s}\,z_{s,n_s}\right)^{\mathrm{T}}$ and $\mathbf{u} = \varepsilon_{T,c}$ (the commanded swivel angle), respectively. The matrices $\mathbf{A}$ and $\mathbf{B}$ are the system and control matrix, respectively, whereas $\mathbf{E}$ is the (coupled) mass matrix.

Due to the different nature of groups of state variables, it makes sense to partition $\mathbf{A}$ and $\mathbf{B}$ into sub-matrices representing the rigid-body motion, the engine dynamics, the flexible-body motion, and the slosh dynamics, thereby identifying the coupling terms between the different sets. The corresponding state-space matrices are then written as:

$$\mathbf{A} = \begin{bmatrix} \mathbf{A_{RR}} & \mathbf{A_{RE}} & \mathbf{A_{RF}} & \mathbf{A_{RS}} \\ \mathbf{A_{ER}} & \mathbf{A_{EE}} & \mathbf{A_{EF}} & \mathbf{A_{ES}} \\ \mathbf{A_{FR}} & \mathbf{A_{FE}} & \mathbf{A_{FF}} & \mathbf{A_{FS}} \\ \mathbf{A_{SR}} & \mathbf{A_{SE}} & \mathbf{A_{SF}} & \mathbf{A_{SS}} \end{bmatrix} \quad \text{and} \quad \mathbf{B} = \begin{pmatrix} \mathbf{B_R} \\ \mathbf{B_E} \\ \mathbf{B_F} \\ \mathbf{B_S} \end{pmatrix} \tag{3}$$

where the indices indicate

1. R for the rigid-body states angle of attack, α, pitch angle, θ, and pitch rate, q;
2. E for the engine states $\ddot{\varepsilon}_T$ (angular acceleration), $\dot{\varepsilon}_T$ (angular velocity) and ε_T (the angular position or swivel angle). These states originate from the assumption that the engine is modelled as an electro-hydraulic servo system, represented by a third-order transfer function;
3. F for the flexible-body states $\dot{\eta}_i$ and η_i for mode i. The total number of states in this group depends on how many bending modes n_f are taken into account;
4. S for the slosh-mass states $\dot{z}_{s,j}$ and $z_{s,j}$ for slosh mass j. The total number of states in this group is given by n_s, *i.e.,* the product of the number of slosh masses and modes per mass.

For the non-linear controller design to be discussed in the next section, we reformulate the above state-space system, and group some of the coupling effects and the engine dynamics. The error-dynamic model is now written in the following form:[12]

$$\begin{aligned}
&\ddot{\theta} - \frac{1}{I_{yy}} \sum_{j=1}^{2} m_{s,j} \ell_{s,j} \ddot{z}_{s,j} = f_q(t, \mathbf{x}, u) + \frac{T - D}{m I_{yy}} \sum_{j=1}^{n_s} m_{s,j} z_{s,j} \\
&\ddot{z}_{s,j} + u_0 \dot{\alpha} - \ell_{s,j} \dot{q} + \sum_{i=1}^{n_f} \phi_i(x_{s,j}) \ddot{\eta}_i = \frac{T - D}{m} \theta - 2\zeta_{s,j} \omega_{s,j} \dot{z}_{s,j} - \omega_{s,j}^2 z_{s,j} \\
&\dot{\alpha} + \frac{1}{m u_0} \sum_{j=1}^{2} m_{s,j} \ddot{z}_{s,j} = f_\alpha(t, \mathbf{x}, u, \alpha_{\text{dis}}) \\
&\ddot{\eta}_i + \sum_{j=1}^{2} m_{s,j} \phi_i(x_{s,j}) \ddot{z}_{s,j} = f_\eta(t, \mathbf{x}, u)
\end{aligned} \tag{4}$$

In the above equation, θ and α represent the rigid-body states of the launch vehicle. The slosh dynamics is modelled as two mass-spring-damping systems (the primary mode for each tank in the first stage), where $m_{s,j}$ represents the slosh mass, $\omega_{s,j}$ and $\zeta_{s,j}$ are the eigenfrequency and damping ratio of the j^{th} slosh mode, and $z_{s,j}$ is the (position) state for the j^{th} slosh mode. T and D denote the total thrust and drag, respectively, whereas α_{dis} in f_α represents the angle of attack induced by external atmospheric disturbances (include discrete gusts and turbulence). Finally, η_i is the generalised coordinate of the i^{th} flexible mode, and the coupling between flexible and slosh modes is enforced through the modal shape function, ϕ_i, at the axial slosh location $x_{s,j}$.

III. Control Design

This paper aims at simultaneously achieving different control objectives using a single control input u. First of all, the controller should guarantee the stability of the closed-loop system. Then, the controller aims at driving θ towards its reference θ_c. The slosh dynamics should also be damped. Finally, the controller should be able to reject external disturbances and be robust to model uncertainties.

To begin with, $f_q(t, \mathbf{x}, u)$ in Eq. (4) is explicitly written as

$$f_q(t, \mathbf{x}, u) = \frac{C_{m_q} \bar{q} S_{\text{ref}} d_{\text{ref}}}{I_{yy}} q + \frac{C_{m_\alpha} \bar{q} S_{\text{ref}} d_{\text{ref}}}{I_{yy}} \alpha + \sum_{i=1}^{n_f} a_{q,\dot{\eta}_j} \dot{\eta}_j + \sum_{i=1}^{n_f} a_{q,\eta_j} \eta_j + \frac{L_e T}{I_{yy}} u \tag{5}$$

with $\bar{q}$ being the dynamic pressure, and $u = \varepsilon_{T,c}$ the commanded swivel angle, the only control input to the system.

Denote the acceleration along the elastic axis as $a_x = \frac{T-D}{m}$, using Eqs. (4) and (5), the dynamics of the launch vehicle are expressed as

$$\begin{bmatrix} 1 & -\frac{m_{s,1}\ell_{s,1}}{I_{yy}} & \cdots & -\frac{m_{s,n_s}\ell_{s,n_s}}{I_{yy}} \\ -\ell_{s,1} & 1+\frac{m_{s,1}}{m} & \cdots & \frac{m_{s,n_s}}{m} \\ \vdots & & \ddots & \\ -\ell_{s,n_s} & \frac{m_{s,1}}{m} & \cdots & 1+\frac{m_{s,n_s}}{m} \end{bmatrix} \begin{pmatrix} \ddot{\theta} \\ \ddot{z}_{s,1} \\ \vdots \\ \ddot{z}_{s,n_s} \end{pmatrix} = \begin{bmatrix} \frac{C_{m_q}\bar{q}S_{\text{ref}}d_{\text{ref}}}{I_{yy}} & 0 & \cdots & 0 \\ 0 & -2\zeta_{s,1}\omega_{s,1} & \cdots & 0 \\ \vdots & & \ddots & \\ 0 & 0 & \cdots & -2\zeta_{s,n_s}\omega_{s,n_s} \end{bmatrix} \begin{pmatrix} \dot{\theta} \\ \dot{z}_{s,1} \\ \vdots \\ \dot{z}_{s,n_s} \end{pmatrix}$$
$$+ \begin{bmatrix} 0 & \frac{a_x m_{s,1}}{I_{yy}} & \cdots & \frac{a_x m_{s,n_s}}{I_{yy}} \\ a_x & -\omega_{s,1}^2 & \cdots & 0 \\ \vdots & & \ddots & \\ a_x & 0 & \cdots & -\omega_{s,n_s}^2 \end{bmatrix} \begin{pmatrix} \theta \\ z_{s,1} \\ \vdots \\ z_{s,n_s} \end{pmatrix} + \begin{pmatrix} \frac{L_e T}{I_{yy}} \\ 0 \\ \vdots \\ 0 \end{pmatrix} u + \begin{pmatrix} \frac{C_{m_\alpha}\bar{q}S_{\text{ref}}d_{\text{ref}}}{I_{yy}}\alpha + \sum_{i=1}^{n_f} a_{q,\dot{\eta}_j}\dot{\eta}_j + \sum_{i=1}^{n_f} a_{q,\eta_j}\eta_j \\ -u_0 f_\alpha - \sum_{i=1}^{n_f}\phi_i(x_{s,j})\ddot{\eta}_i \\ \vdots \\ -u_0 f_\alpha - \sum_{i=1}^{n_f}\phi_i(x_{s,j})\ddot{\eta}_i \end{pmatrix} \tag{6}$$

Equation (6) can be written in a condensed form as

$$\mathbf{M_s}\ddot{\mathbf{x}} = -\mathbf{C_s}\dot{\mathbf{x}} - \mathbf{K_s}\mathbf{x} + \mathbf{B}_s u + \mathbf{d}_s \tag{7}$$

The state vector is defined as $\mathbf{x} = [\theta, z_{s,1}, z_{s,2}, \ldots, z_{s,n_s}]^{\mathrm{T}}$. Since $0 < m_{s,j} < m$ for all j, the mass matrix $\mathbf{M}_s$ in Eq. (7) is always invertible. The non-zero off-diagonal elements of $\mathbf{M}_s$ reflect the inertial couplings between the pitch and slosh dynamics. From Eq. (7), the launch vehicle pitch dynamics is written as

$$\ddot{\theta} = f_\theta(\dot{\theta}, \theta, \dot{z}_{s,j}, z_{s,j}) + Gu + d_\theta \tag{8}$$

in which f_θ represents the first row of $\mathbf{M_s}^{-1}(-\mathbf{C_s}\dot{\mathbf{x}} - \mathbf{K_s}\mathbf{x})$, while d_θ represents the first row of $\mathbf{M_s}^{-1}\mathbf{d}_s$ in Eq. (7). The control effectiveness G equals the first row of $\mathbf{M_s}^{-1}\mathbf{B}_s$.

Assumption 1 *G is non-singular for all t.*

A. Partial Feedback Linearisation

The dynamic system given in Eq. (6) contains coupled rigid-body pitch and slosh dynamics. However, there is only one single control input to the system. Therefore, the control problem of simultaneously stabilising θ and slosh states becomes an under-actuated problem. Since rigid-body motion control has higher priority, the controlled output variable is selected as $y = \theta$. The resulting system input-output mapping can be linearised using the following control input:

$$u = (\nu - \hat{f}_\theta)/\hat{G} \tag{9}$$

in which $\hat{f}_\theta$ and $\hat{G}$ represent the estimations of f_θ and G in Eq. (8). ν in Eq. (9) is a virtual control input, which will be designed later for stabilising the linearised dynamics. Moreover, slosh dynamics is not used in Eq. (9), thus the system dynamics is only partially linearised (from u to θ), while the slosh dynamics remains unchanged. Substituting Eq. (9) into Eq. (8), the closed-loop dynamics is

$$\ddot{\theta} = f_\theta(\dot{\theta}, \theta, \dot{z}_{s,j}, z_{s,j}) + G(\nu - \hat{f}_\theta)/\hat{G} + d_\theta = \nu + (f_\theta - \hat{f}_\theta) + (G - \hat{G})u + d_\theta \triangleq \nu + \varepsilon_{\text{ndi}} \tag{10}$$

It can be observed from Eq. (10) that if the system dynamics is known accurately, and if there is no external disturbance, then the partial feedback linearisation results in perfect $\ddot{\theta} = \nu$, which is a double integral system. However, model uncertainties and external disturbances are inevitable in practice, resulting in the lumped uncertainty term ε_{ndi} in Eq. (10). In light-perturbation circumstances, where ε_{ndi} is bounded, a linear virtual control design can still ensure the boundedness of the tracking error. However, in severe perturbation cases where ε_{ndi} becomes unbounded, the stability of the closed-loop system is not guaranteed anymore. The sensitivity of feedback linearisation to model uncertainties and external disturbances is one of its main drawbacks.

In view of the major drawback of the model-based feedback linearisation, the sensor-based Incremental Non-linear Dynamic Inversion (INDI) was proposed in Ref. 24. Recently, INDI was generalised to generic multi-input/multi-output non-linear systems.[25] The partial input-output feedback linearisation can also be achieved by INDI. Denote the sampling interval as Δt. Taking the first-order Taylor series expansion of Eq. (8) around the condition at $t-\Delta t$ (denoted by the subscript 0) results in

$$\begin{aligned}\ddot{\theta} &= f_\theta(\dot{\theta},\theta,\dot{z}_{s,j},z_{s,j}) + Gu + d_\theta \\ &= \ddot{\theta}_0 + \frac{\partial f_\theta}{\partial \dot{\theta}}\bigg|_0 \Delta\dot{\theta} + \frac{\partial f_\theta}{\partial \theta}\bigg|_0 \Delta\theta + \sum_{j=1}^{n_s}\frac{\partial f_\theta}{\partial \dot{z}_{s,j}}\bigg|_0 \Delta\dot{z}_{s,j} + \sum_{j=1}^{n_s}\frac{\partial f_\theta}{\partial z_{s,j}}\bigg|_0 \Delta z_{s,j} + G_0\Delta u + \Delta d_\theta + R_1 \qquad (11)\end{aligned}$$

where $\Delta(\cdot)$ represents the variations of $(\cdot)$ in one sampling interval Δt. R_1 in Eq. (11) is the expansion remainder, which Lagrange form is

$$R_1 = \frac{1}{2}\left(\frac{\partial^2 f_\theta}{\partial\dot{\theta}^2}\bigg|_m \Delta\dot{\theta}^2 + \frac{\partial^2 f_\theta}{\partial\theta^2}\bigg|_m \Delta\theta^2 + \sum_{j=1}^{n_s}\frac{\partial^2 f_\theta}{\partial \dot{z}_{s,j}^2}\bigg|_m \Delta\dot{z}_{s,j}^2 + \sum_{j=1}^{n_s}\frac{\partial^2 f_\theta}{\partial z_{s,j}^2}\bigg|_m \Delta z_{s,j}^2\right) \qquad (12)$$

in which $(\cdot)|_m$ means evaluating $(\cdot)$ at a condition where $x\in[x(t-\Delta t),x(t)]$, $\dot{x}\in[\dot{x}(t-\Delta t),\dot{x}(t)]$, and $u\in[u(t-\Delta t),u(t)]$. The incremental control is designed as

$$\Delta u = (\nu - \ddot{\theta}_0)/\hat{G}_0 \qquad (13)$$

The actual actuator control command equals

$$u = u_0 + \Delta u \qquad (14)$$

where u_0 is the control input at $t-\Delta t$. Substituting Eq. (13) into Eq. (11) leads to

$$\begin{aligned}\ddot{\theta} &= \nu + (G_0-\hat{G}_0)\Delta u + \Delta d_\theta + \left(\frac{\partial f_\theta}{\partial \dot{\theta}}\bigg|_0 \Delta\dot{\theta} + \frac{\partial f_\theta}{\partial \theta}\bigg|_0 \Delta\theta + \sum_{j=1}^{n_s}\frac{\partial f_\theta}{\partial \dot{z}_{s,j}}\bigg|_0 \Delta\dot{z}_{s,j} + \sum_{j=1}^{n_s}\frac{\partial f_\theta}{\partial z_{s,j}}\bigg|_0 \Delta z_{s,j} + R_1\right) \\ &= \nu + (G_0-\hat{G}_0)\Delta u + \Delta d_\theta + \left(\frac{\partial f_\theta}{\partial \dot{\mathbf{x}}}\bigg|_0 \Delta\dot{\mathbf{x}} + \frac{\partial f_\theta}{\partial \mathbf{x}}\bigg|_0 \Delta\mathbf{x} + \frac{1}{2}\frac{\partial^2 f_\theta}{\partial\dot{\mathbf{x}}^2}\bigg|_m \Delta\dot{\mathbf{x}}^2 + \frac{1}{2}\frac{\partial^2 f_\theta}{\partial\mathbf{x}^2}\bigg|_m \Delta\mathbf{x}^2\right) \\ &\triangleq \nu + (G_0-\hat{G}_0)\Delta u + \Delta d_\theta + \delta(\mathbf{x},\dot{\mathbf{x}},t) \triangleq \nu + \varepsilon_{\text{indi}} \qquad (15)\end{aligned}$$

In Eq. (15), $\delta(\mathbf{x},\dot{\mathbf{x}},t)$ represents the closed-loop value of the state variations and expansion remainders. $\varepsilon_{\text{indi}}$ is the lumped uncertainty term under INDI control.

Assumption 2 *The lumped variation term $\delta(\mathbf{x},\dot{\mathbf{x}},t)$ in Eq. (15) satisfies $|\delta(\mathbf{x},\dot{\mathbf{x}},t)|\le\bar{\delta}$.*

In view of Eq. (6), $\mathbf{x}$ is twice continuously differentiable. Therefore, $\lim_{\Delta t\to 0}\|\Delta\mathbf{x}\|_2 = 0$ and $\lim_{\Delta t\to 0}\|\Delta\dot{\mathbf{x}}\|_2 = 0$. If the first-order and second-order partial derivatives of f_θ with respect to $\mathbf{x}$ and $\dot{\mathbf{x}}$ are bounded, then it can be seen from Eq. (15) that the absolute value of $\delta(\mathbf{x},\dot{\mathbf{x}},t)$ approaches zero as Δt decreases. Therefore, this assumption can be met by the selection of a sufficiently small sampling interval.

Proposition 1 *Under Assumptions 1 and 2, if $|1-G/\hat{G}|\le\bar{b}<1$ for all t, then for sufficiently small sampling interval Δt, the residual error ε_{indi} in Eq. (15) is ultimately bounded.*

Proof: Recall Eq. (15), $\ddot{\theta}=\nu+\varepsilon_{\text{indi}}$. This equation is valid at every time step, thus at $t-\Delta t$, $\ddot{\theta}_0=\nu_0+\varepsilon_{\text{indi},0}$. Using this relationship and Eqs. (13) and (15), the residual error $\varepsilon_{\text{indi}}$ is further derived as

$$\begin{aligned}\varepsilon_{\text{indi}} &= \delta(\mathbf{x},\dot{\mathbf{x}},t) + \Delta d_\theta + (G_0-\hat{G}_0)\Delta u = \delta(\mathbf{x},\dot{\mathbf{x}},t) + \Delta d_\theta + (G_0-\hat{G}_0)\hat{G}_0^{-1}(\nu-\ddot{\theta}_0) \\ &= \delta(\mathbf{x},\dot{\mathbf{x}},t) + \Delta d_\theta + ((G\hat{G}^{-1})|_0 - 1)(\nu-\nu_0-\varepsilon_{\text{indi},0}) \\ &\triangleq E\varepsilon_{\text{indi},0} - E(\nu-\nu_0) + \delta(\mathbf{x},\dot{\mathbf{x}},t) + \Delta d_\theta \qquad (16)\end{aligned}$$

To avoid the chattering phenomenon, the virtual control ν is designed to be continuous in time. Using this continuity, $\lim_{\Delta t\to 0}|\nu-\nu_0|=0$. This also indicates that there always exists a Δt such that $\nu-\nu_0$ is bounded by a constant $\overline{\Delta\nu}$. In practice, the variation of external disturbance in one incremental time step is bounded, thus the bound of Δd_θ is denoted as $\overline{\Delta d}$. Given these bounded variation terms, Eq. (16) is in a similar form with Eq. (14) in Ref. 19. Therefore, analogous to the proof of Theorem 1 in Ref. 19, $\varepsilon_{\text{indi}}$ is bounded at each time step and is ultimately bounded by $(\overline{\Delta\nu}\bar{b} + \bar{\delta} + \overline{\Delta d})/(1 - \bar{b})$. □

Although the term "sufficiently small" sampling interval is used in Proposition 1, it is not difficult to find a practical sampling frequency. 100 Hz is sufficient for rigid aircraft, which has been verified by real-world flight tests.[26]

B. Virtual Control Design

After using the model-based partial feedback linearisation, or the sensor-based INDI, the pitch dynamics become $\ddot{\theta} = \nu + \varepsilon_{\text{ndi/indi}}$ (Eqs. (10, 15)). In conventional INDI control, the following virtual control design is used to stabilise the tracking error of θ:

$$\nu_{\text{indi}} = \ddot{\theta}_{\text{ref}} - k_\theta(\theta - \theta_{\text{ref}}) - k_q(q - q_{\text{ref}}) \tag{17}$$

where k_θ and k_q are positive control gains. However, this virtual control design only contains rigid-body state feedback, thus it is not sufficient to damp out slosh motions. This has been demonstrated by the simulation results in Ref. 13. To simultaneously achieve rigid-body state tracking and slosh suppression, the incremental sliding mode control (INDI-SMC) will be used. Recall Eq. (6), the complete system dynamics after partial feedback linearisation can be written in the state-space form as

$$\begin{pmatrix} \ddot{\theta} \\ \dot{\theta} \\ \ddot{z}_{s,1} \\ \dot{z}_{s,1} \\ \vdots \\ \ddot{z}_{s,n_s} \\ \dot{z}_{s,n_s} \end{pmatrix} = \begin{bmatrix} 0 & 0 & 0 & 0 & \dots & 0 & 0 \\ 1 & 0 & 0 & 0 & \dots & 0 & 0 \\ a_{1,1} & a_{1,2} & a_{1,3} & a_{1,4} & \dots & a_{1,2n_s+1} & a_{1,2n_s+2} \\ 0 & 0 & 1 & 0 & \dots & 0 & 0 \\ \vdots & \vdots & \vdots & \vdots & & \vdots & \vdots \\ a_{n_s,1} & a_{n_s,2} & a_{n_s,3} & a_{n_s,4} & \dots & a_{n_s,2n_s+1} & a_{n_s,2n_s+2} \\ 0 & 0 & 0 & 0 & \dots & 1 & 0 \end{bmatrix} \begin{pmatrix} \dot{\theta} \\ \theta \\ \dot{z}_{s,1} \\ z_{s,1} \\ \vdots \\ \dot{z}_{s,n_s} \\ z_{s,n_s} \end{pmatrix} + \begin{pmatrix} 1 \\ 0 \\ b_1 \\ 0 \\ \vdots \\ b_{n_s} \\ 0 \end{pmatrix} \nu + \begin{pmatrix} \varepsilon_{\text{ndi/indi}} \\ 0 \\ d_1 \\ 0 \\ \vdots \\ d_{n_s} \\ 0 \end{pmatrix} \tag{18}$$

The virtual control ν becomes the new control input of this system, and it should be designed to fulfill the tracking task, damp out the slosh dynamics, and enhance the robustness against model uncertainties and external disturbances. Theses tasks can be achieved by sliding mode control.

Define the new state vector as $\mathbf{X} = [\dot{\theta}, \theta, \dot{z}_{s,1}, z_{s,1}, \dots, \dot{z}_{s,n_s}, z_{s,n_s}]^{\mathrm{T}}$, and define its reference vector as $\mathbf{X}_{\text{ref}} = [\dot{\theta}_{\text{ref}}, \theta_{\text{ref}}, 0, 0, \dots, 0, 0]^{\mathrm{T}}$, then the dynamics of the tracking error $\mathbf{e} = \mathbf{X} - \mathbf{X}_{\text{ref}}$ are written as

$$\dot{\mathbf{e}} = \mathbf{A}\mathbf{X} + \mathbf{B}\nu + \mathbf{d} - \dot{\mathbf{X}}_{\text{ref}} = \hat{\mathbf{A}}\mathbf{X} + \hat{\mathbf{B}}\nu + (\mathbf{A} - \hat{\mathbf{A}})\mathbf{X} + (\mathbf{B} - \hat{\mathbf{B}})\nu + \mathbf{d} - \dot{\mathbf{X}}_{\text{ref}} \tag{19}$$

where only the estimated $\hat{\mathbf{A}}$ and $\hat{\mathbf{B}}$ are available for control-system design. The model uncertainties and external disturbances in Eqs. (18) and (19) can be classified into matched and unmatched uncertainties. Because $\varepsilon_{\text{ndi/indi}}$ enters the state equation at the same point as the virtual control input ν, it is a matched uncertainty term. Although sliding mode control has inherent robustness to matched uncertainties, the sliding surface should be carefully designed to ensure the robustness to unmatched uncertainties, which in this case, are the uncertain system elements $a_{i,j},\ i = 1, ..., n_s,\ j = 1, ..., 2n_s + 2,\ b_1, ..., b_{n_s}$, and $d_1, ..., d_{n_s}$.

Design the sliding surface as $s = \mathbf{C}^{\mathrm{T}}\mathbf{e} = 0$, where $\mathbf{C} \in \mathbb{R}^{(2n_s+2)\times 1}$. This vector $\mathbf{C}$ is designed such that the unmatched uncertainties belong to the *null space* of $\mathbf{C}^{\mathrm{T}}$, while $\mathbf{C}^{\mathrm{T}}\hat{\mathbf{B}}$ should still be invertible. In this paper, $\mathbf{C}$ is designed as

$$\mathbf{C} = [1, c_\theta, 0, c_1, \dots, 0, c_{n_s}]^{\mathrm{T}} \tag{20}$$

Using Eqs. (18) and (20), the following equations can be verified

$$\mathbf{C}^{\mathrm{T}}(\mathbf{A} - \hat{\mathbf{A}}) = \mathbf{0},\quad \mathbf{C}^{\mathrm{T}}(\mathbf{B} - \hat{\mathbf{B}}) = 0,\quad \mathbf{C}^{\mathrm{T}}\hat{\mathbf{B}} = 1,\quad \mathbf{C}^{\mathrm{T}}\mathbf{d} = \varepsilon_{\text{ndi/indi}} \tag{21}$$

Lemma 1 (Ref. 23) *If a Lyapunov function V satisfies $\dot{V} + \alpha V + \beta V^\gamma \le 0,\ \alpha, \beta > 0,\ 0 < \gamma < 1$, then $V = 0$ will be reached in finite time $T \le \frac{1}{\alpha(1-\gamma)} \ln \frac{\alpha V^{1-\gamma}(t_0) + \beta}{\beta}$.*

Theorem 1 *For the system modeled by Eq. (18) with sliding surface $s = \mathbf{C}^{\mathrm{T}}\mathbf{e} = 0$, where $\mathbf{C}$ is given by Eq. (20), design $\nu = -k_1 s - k_2|s|^{\rho}sign(s) - \mathbf{C}^{\mathrm{T}}\hat{\mathbf{A}}\mathbf{X} + \mathbf{C}^{\mathrm{T}}\dot{\mathbf{X}}_{ref}$, $k_1 > 0, k_2 > \eta > 0, 0 < \rho < 1$, then*

1. *In the absence of the perturbation term $\varepsilon_{ndi/indi}$, $s = 0$ is reached in finite time.*
2. *If the perturbation term $\varepsilon_{ndi/indi}$ is bounded, then the system trajectories will converge to the neighbourhood of $s = 0$ as $s \leq \bar{s}_{ndi/indi} = (|\varepsilon_{ndi/indi}|/(k_2 - \eta))^{\frac{1}{\rho}}$ in finite time.*

Proof: Consider a candidate Lyapunov function $V = \frac{1}{2}s^2$, using Eqs. (19) and (21), the time derivative of V yields

$$\begin{aligned}
\dot{V} &= s[\mathbf{C}^{\mathrm{T}}(\hat{\mathbf{A}}\mathbf{X} + \hat{\mathbf{B}}\nu + (\mathbf{A} - \hat{\mathbf{A}})\mathbf{X} + (\mathbf{B} - \hat{\mathbf{B}})\nu + \mathbf{d} - \dot{\mathbf{X}}_{\mathrm{ref}})] \\
&= s[\mathbf{C}^{\mathrm{T}}\hat{\mathbf{A}}\mathbf{X} + \nu + \varepsilon_{\mathrm{ndi/indi}} - \mathbf{C}^{\mathrm{T}}\dot{\mathbf{X}}_{\mathrm{ref}})] \\
&= -k_1 s^2 - k_2|s|^{\rho+1} + s\varepsilon_{\mathrm{ndi/indi}}
\end{aligned} \tag{22}$$

1. When $\varepsilon_{\mathrm{ndi/indi}} = 0$, Eq. (22) is derived as

$$\dot{V} = -k_1 s^2 - k_2|s|^{\rho+1} = -2k_1 V - 2^{(\rho+1)/2}k_2 V^{(\rho+1)/2} \tag{23}$$

   Using Lemma 1, V converges to zero in finite time:

$$T \leq \ln[(k_1 V(t_0))^{(1-\rho)/2} + 2^{(\rho-1)/2}k_2)/(2^{(\rho-1)/2}k_2)]/[k_1(1-\rho)]$$

   Equivalently, $s = 0$ is reached in finite time.

2. When $\varepsilon_{\mathrm{ndi/indi}} \neq 0$, Eq. (22) is derived as

$$\dot{V} \leq -k_1 s^2 - k_2|s|^{\rho+1} + |s||\varepsilon_{\mathrm{ndi/indi}}| \leq -k_1 s^2 - \eta|s|^{\rho+1}, \quad \forall|s| \geq \left(\frac{|\varepsilon_{\mathrm{ndi/indi}}|}{k_2 - \eta}\right)^{\frac{1}{\rho}} \triangleq \bar{s}_{\mathrm{ndi/indi}} \tag{24}$$

   Using Lemma 1, the above equation demonstrates that s converges to the domain $s \leq \bar{s}_{\mathrm{ndi/indi}}$ in finite time. □

It is noteworthy that the sliding surface designed in this paper guarantees that all the unmatched uncertainties belong to the null space of $\mathbf{C}^{\mathrm{T}}$, and the resulting dynamics are only perturbed by $\varepsilon_{\mathrm{ndi/indi}}$, which lies in the input channel of ν. In theory, this matched uncertainty term can be completely cancelled in finite time using the conventional $\eta-$ reaching law, which would result in $\dot{V} = s(-k_s\mathrm{sign}(s) + \varepsilon_{\mathrm{ndi/indi}}) \leq -\eta|s|, \ \ \forall k_s \geq \eta + |\varepsilon_{\mathrm{ndi/indi}}|$. However, this reaching law contains the discontinuous sign function, which causes chattering in practice. If the boundary-layer approximation is used, the sliding variable s would also stay in the vicinity of its origin. Moreover, the finite-time convergence property would also lost. By contrast, the fast terminal sliding mode reaching law $-k_1 s - k_2|s|^{\rho}\mathrm{sign}(s)$ is adopted in this paper. The choice $0 < \rho < 1$ ensures the achievement of finite-time reaching and continuity at the same time.

The ultimate bound of s can be diminished by increasing k_2 and reducing ρ (given $|\varepsilon_{\mathrm{ndi/indi}}|/(k_2 - \eta) < 1$). Although the nominal model $\hat{\mathbf{A}}$ is needed in ν, using Eqs. (18) and (20), it can be seen that $\mathbf{C}^{\mathrm{T}}\hat{\mathbf{A}} = [c_\theta, 0, c_1, 0, ..., c_{n_s}, 0]$, which actually does not contain any model information.

On the sliding surface, the equivalent virtual control is $\nu_{\mathrm{eq}} = -\mathbf{C}^{\mathrm{T}}\hat{\mathbf{A}}\mathbf{X} + \mathbf{C}^{\mathrm{T}}\dot{\mathbf{X}}_{\mathrm{ref}}$, which is calculated by substituting $s = 0$ into the ν given in Theorem 1. Therefore, the equivalent closed-loop dynamics is

$$\dot{\mathbf{e}} = \mathbf{A}\mathbf{X} + \mathbf{B}\nu + \mathbf{d} - \dot{\mathbf{X}}_{\mathrm{ref}} = \mathbf{A}\mathbf{X} + \mathbf{B}(-\mathbf{C}^{\mathrm{T}}\hat{\mathbf{A}}\mathbf{X} + \mathbf{C}^{\mathrm{T}}\dot{\mathbf{X}}_{\mathrm{ref}}) + \mathbf{d} - \dot{\mathbf{X}}_{\mathrm{ref}} \tag{25}$$

Since $\mathbf{C}^{\mathrm{T}}(\mathbf{A} - \hat{\mathbf{A}}) = \mathbf{0}$ (Eq. (21)), then

$$\dot{\mathbf{e}} = (\mathbf{I} - \mathbf{B}\mathbf{C}^{\mathrm{T}})\mathbf{A}\mathbf{X} - (\mathbf{I} - \mathbf{B}\mathbf{C}^{\mathrm{T}})\dot{\mathbf{X}}_{\mathrm{ref}} + \mathbf{d} \tag{26}$$

Consider θ_{ref} as a piecewise linear signal such that $\ddot{\theta}_{\mathrm{ref}} = 0$. Because $\mathbf{X}_{\mathrm{ref}} = [\dot{\theta}_{\mathrm{ref}}, \theta_{\mathrm{ref}}, 0, 0, \ldots, 0, 0]^{\mathrm{T}}$, using Eq. (18), it can be seen that $\dot{\mathbf{X}}_{\mathrm{ref}} = \mathbf{A}\mathbf{X}_{\mathrm{ref}}$. Substituting this equation into Eq. (26) yields

$$\dot{\mathbf{e}} = (\mathbf{I} - \mathbf{B}\mathbf{C}^{\mathrm{T}})\mathbf{A}\mathbf{e} + \mathbf{d} \triangleq \mathbf{A}_{\mathrm{e}}\mathbf{e} + \mathbf{d} \tag{27}$$

Although $\mathbf{A}_\mathrm{e} \in \mathbb{R}^{(2n_s+2)\times(2n_s+2)}$, it can be examined that the rank of $\mathbf{A}_e$ equals $2n_s+1$. This shows that on the sliding surface, the closed-loop system behaves as its reduced dynamics. To analyse the stability of the reduced-order dynamics, select $\mathbf{e}_r = \mathbf{T}\mathbf{e}$, where $\mathbf{T} \in \mathbb{R}^{(2n_s+1)\times(2n_s+2)}$, and ensure the rank of $\mathbf{T}$ equals $2n_s+1$. Without loss of generality, select $\mathbf{e}_r = [e_\theta, \dot{z}_{s,1}, z_{s,1}, \ldots, \dot{z}_{s,n_s}, z_{s,n_s}]$, then Eq. (27) can be rewritten as

$$\begin{pmatrix} \dot{e}_{\dot{\theta}} \\ \dot{\mathbf{e}}_r \end{pmatrix} = \begin{bmatrix} A_{11} & \mathbf{A}_{12} \\ \mathbf{A}_{21} & \mathbf{A}_{22} \end{bmatrix} \begin{pmatrix} e_{\dot{\theta}} \\ \mathbf{e}_r \end{pmatrix} + \begin{pmatrix} \varepsilon_{\mathrm{ndi/indi}} \\ \mathbf{d}_r \end{pmatrix} \tag{28}$$

On the sliding surface, $s = \mathbf{C}^\mathrm{T}\mathbf{e} = [1, c_\theta, 0, c_1, \ldots, 0, c_{n_s}]\mathbf{e} = 0$. Therefore, $e_{\dot{\theta}} = -[c_\theta, 0, c_1, \ldots, 0, c_{n_s}]\mathbf{e}_r$. Substituting this relationship into Eq. (28), the reduced-order dynamics is

$$\dot{\mathbf{e}}_r = \mathbf{A}_{22}\mathbf{e}_r - \mathbf{A}_{21}[c_\theta, 0, c_1, \ldots, 0, c_{n_s}]\mathbf{e}_r + \mathbf{d}_r \triangleq \mathbf{A}_{rr}\mathbf{e}_r + \mathbf{d}_r \tag{29}$$

Recall Eq. (6), $\mathbf{d}_r$ contains the aerodynamic force f_α and the elastic perturbations. A part of these perturbations vanishes at the origin ($\alpha = q = z_{s,j} = \eta_i = 0$), while the remaining terms caused by the disturbing angle of attack α_dis are non-vanishing perturbations. In view of this, the following assumption is made:

Assumption 3 *In Eq. (29)* $\|\mathbf{d}_r\|_2 \leq \gamma_d \|\mathbf{e}_r\|_2 + \varepsilon_d$.

Theorem 2 *Under Assumption 3, if* $\mathbf{C}$ *in Eq. (20) is designed such that* $\mathbf{A}_{rr}$ *in Eq. (29) is Hurwitz, and if* $\gamma_d < \frac{1}{2\|\mathbf{P}\|_2}$, *where* $\mathbf{P} = \mathbf{P}^\mathrm{T} > 0$ *is the solution of the Lyapunov function* $\mathbf{P}\mathbf{A}_{rr} + \mathbf{A}_{rr}^\mathrm{T}\mathbf{P} = -\mathbf{I}$, *then on the sliding surface* $s = \mathbf{C}^\mathrm{T}\mathbf{e} = 0$, *the tracking error vector* $\mathbf{e}$ *in Eq. (19) is ultimately bounded.*

Proof: Consider a candidate Lyapunov function $V_e = \mathbf{e}_r^\mathrm{T}\mathbf{P}\mathbf{e}_r$, using Eq. (29), the time derivative of V_e is

$$\begin{aligned} \dot{V}_e &= \mathbf{e}_r^\mathrm{T}(\mathbf{P}\mathbf{A}_{rr} + \mathbf{A}_{rr}^\mathrm{T}\mathbf{P})\mathbf{e}_r + 2\mathbf{e}_r^\mathrm{T}\mathbf{P}\mathbf{d}_r \\ &\leq -\|\mathbf{e}_r\|_2^2 + 2\|\mathbf{e}_r\|_2\|\mathbf{P}\|_2\|\mathbf{d}_r\|_2 \leq -\|\mathbf{e}_r\|_2^2 + 2\gamma_d\|\mathbf{P}\|_2\|\mathbf{e}_r\|_2^2 + 2\varepsilon_d\|\mathbf{P}\|_2\|\mathbf{e}_r\|_2 \\ &\leq -(1-\sigma_1)\|\mathbf{e}_r\|_2^2 + 2\varepsilon_d\|\mathbf{P}\|_2\|\mathbf{e}_r\|_2 \leq -(1-\sigma_1)(1-\sigma_2)\|\mathbf{e}_r\|_2^2, \quad \forall \|\mathbf{e}_r\|_2 \geq \frac{2\varepsilon_d\|\mathbf{P}\|_2}{(1-\sigma_1)\sigma_2} \end{aligned} \tag{30}$$

in which $\sigma_1 \in (0,1)$ is chosen close enough to one such that $\gamma_d < \frac{\sigma_1}{2\|\mathbf{P}\|_2}$. σ_2 is also chosen within the interval $(0,1)$. Apply the Theorem 4.18 in Ref. 22, it is concluded that $\mathbf{e}_r$ is ultimately bounded by $\frac{2\varepsilon_d\|\mathbf{P}\|_2}{(1-\sigma_1)\sigma_2}\sqrt{\frac{\lambda_{\max}(\mathbf{P})}{\lambda_{\min}(\mathbf{P})}}$, in which $\lambda_{\max}(\mathbf{P})$ and $\lambda_{\min}(\mathbf{P})$ represent the maximum and minimum eigenvalues of $\boldsymbol{P}$, respectively.

Furthermore, on the sliding surface, Eq. (20) leads to $e_{\dot{\theta}} = -[c_\theta, 0, c_1, \ldots, 0, c_{n_s}]\mathbf{e}_r$. Therefore, $e_{\dot{\theta}}$ is ultimately bounded by $\sqrt{c_\theta^2 + c_1^2 + \cdots + c_{n_s}^2}\frac{2\varepsilon_d\|\mathbf{P}\|_2}{(1-\sigma_1)\sigma_2}\sqrt{\frac{\lambda_{\max}(\mathbf{P})}{\lambda_{\min}(\mathbf{P})}}$. As a result, the entire tracking error vector $\mathbf{e}$ in Eq. (19) is ultimately bounded. □

C. Comparisons of INDI, INDI-SMC, and FL-SMC

The main difference between INDI control and INDI-SMC lies in the virtual control design. After the partial feedback linearisation using incremental non-linear dynamic inversion, the closed-loop pitch dynamics is $\ddot{\theta} = \nu + \varepsilon_{\mathrm{ndi/indi}}$. Conventional INDI control only stabilise this rigid-body motion, with ν_indi given in Eq. (17). On the contrary, the virtual control of INDI-SMC is a function of sliding variable s, which is designed to stabilise both rigid-body and slosh dynamics. The inclusion of SMC also robustifies the INDI control, as the matched uncertainty term is completely cancelled on the sliding surface. The INDI-SMC designed in this paper also ensures the robustness against unmatched uncertainties, which is achieved by exploiting the null space in the sliding surface design.

On the other hand, FL-SMC (feedback linearisation or non-linear dynamic inversion-based SMC) and INDI-SMC use the same SMC virtual control design given in Theorem 1, and their differences are in the linearisation loop. As shown in Sec. III.A, FL uses both $\hat{f}_\theta$ and $\hat{G}$ for linearisation, while INDI only needs the estimated control effectiveness $\hat{G}$. A block diagram for INDI-SMC is shown in Fig. 4. Although the model dependency of INDI is less, its robustness is enhanced by virtue of its sensor-based nature.[19] Despite the fact that lumped perturbation terms are present in the closed-loop of feedback linearisation and INDI, ε_ndi and $\varepsilon_\mathrm{indi}$ have different properties. As discussed in Ref. 19, the boundedness conditions on $\varepsilon_\mathrm{indi}$ are easier

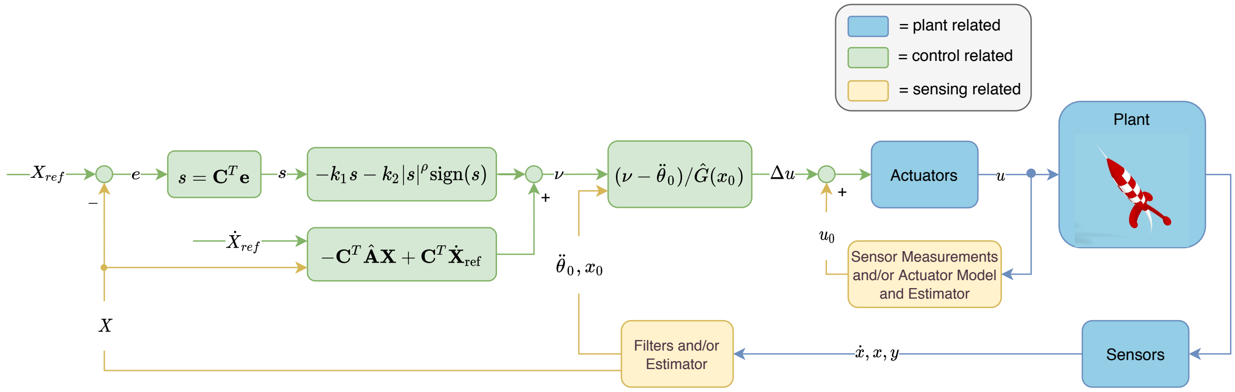

Figure 4. Block diagram for INDI-SMC.

to achieve in practice, while ε_{ndi} can become unbounded in severe fault or damage cases. Moreover, even in the circumstances where both ε_{ndi} and $\varepsilon_{\text{indi}}$ are bounded, there exists a sampling frequency such that the upper bound on $\varepsilon_{\text{indi}}$ is smaller. The smaller bound of $\varepsilon_{\text{indi}}$ can effectively reduce the ultimate bound on the tracking error, and can also reduce the minimum possible gains required by sliding mode controllers and observers.[19] These advantages of INDI-SMC over FL-SMC have been verified by quadrotor flight tests in Ref. 20.

IV. Results and Discussions

A. Nominal Configuration

The analysis of controller performance will be done in several steps, taking previous results as a baseline.[13] The configuration of the plant is that of a rigid-body representation of the launcher, with an LOX and RP-1 tank in the first stage that can exhibit sloshing. The two tanks in the second stage are considered to be completely filled, and are thus assumed to be rigid. The point of interest is that of maximum dynamic pressure, *i.e.,* at $t = 63.5$ s into the launch. Information about the launch trajectory, and the details about the state variables can be found in Ref. 5.

The baseline controller is a state-feedback controller, with gains obtained from optimal-control theory, the so-called Linear Quadratic Regulator (LQR). The LQR has been designed for a relatively smooth response with a maximum state deviation of $\Delta\theta = 1°$, $\Delta q = 5°/\text{s}$, $\Delta\dot{z}_s = 30$ m/s and $\Delta z_s = 40$ m. The latter two large deviations have been selected to avoid a strong controller response due to more violent slosh motion. With a maximum swivel angle of $\Delta\varepsilon_T = 6°$, this gives the gains $\mathbf{K_{lqr}} = (6.07, 1.37, \text{-}0.0045, \text{-}0.0154, \text{-}0.0027, \text{-}0.0148)$, associated with states θ, q, $\dot{z}_{s,1}$, $z_{s,1}$, $\dot{z}_{s,2}$ and $z_{s,2}$. It is noted that the angle of attack is not fed back to the controller. In the current research, we assume perfect rigid- and slosh-state knowledge; the observer developed in Ref. 13 has shown to be working well to provide this slosh knowledge. However, it is left as future work to also include a (rigid-)state observer, *e.g.,* one that works well in the presence of turbulence and other uncertainties.

Finally, to minimise slosh excitation due to discrete command changes, a first-order command pre-filter is included in the pitch-angle channel, with transfer function

$$H_c(s) = \frac{1}{\tau s + 1} \tag{31}$$

where the time constant $\tau = 1.25$ s. This value has not been optimised, but as it reduces the slosh excitation it serves its purpose for this paper.

The manoeuvres that will be executed are step commands in pitch angle, *i.e.,* $\theta_c = 2°$ and $\theta_c = 5°$. An example of the baseline-controller performance is shown in Fig. 5, which shows the response after $\theta_c = 5°$. The coupling between rigid-body motion and the slosh motion is clear, as the oscillating slosh masses induce a perturbing oscillation in the swivel angle and as a very minor oscillation in the pitch motion. Due to the inherent damping in the slosh model, the oscillations slowly damp out. Overall, the response is stable, despite the destabilising LOX mode, which is very well controlled.

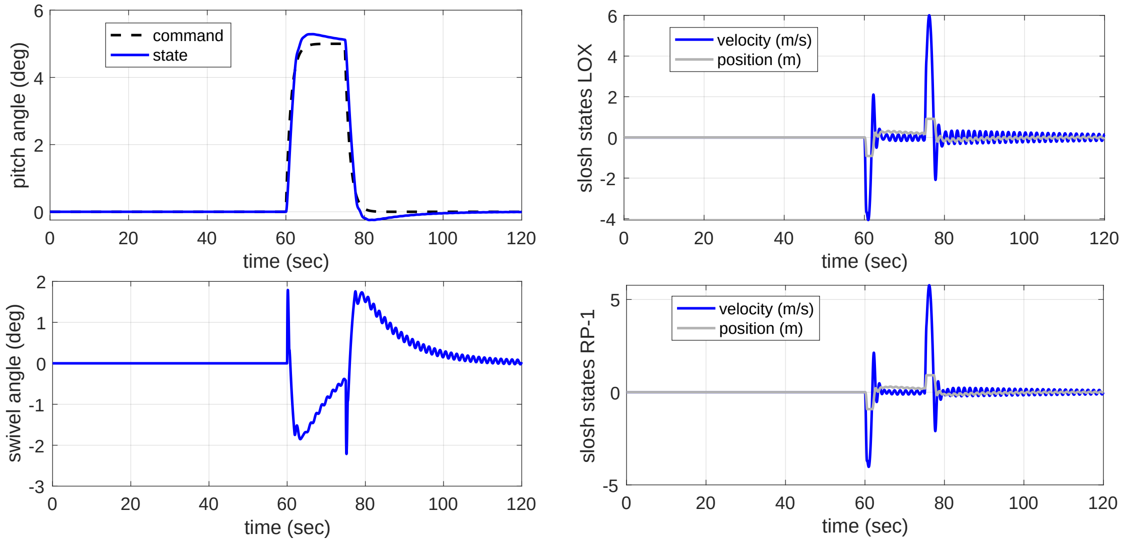

Figure 5. Benchmark performance: $\theta_c = 5°$, LQR controller.

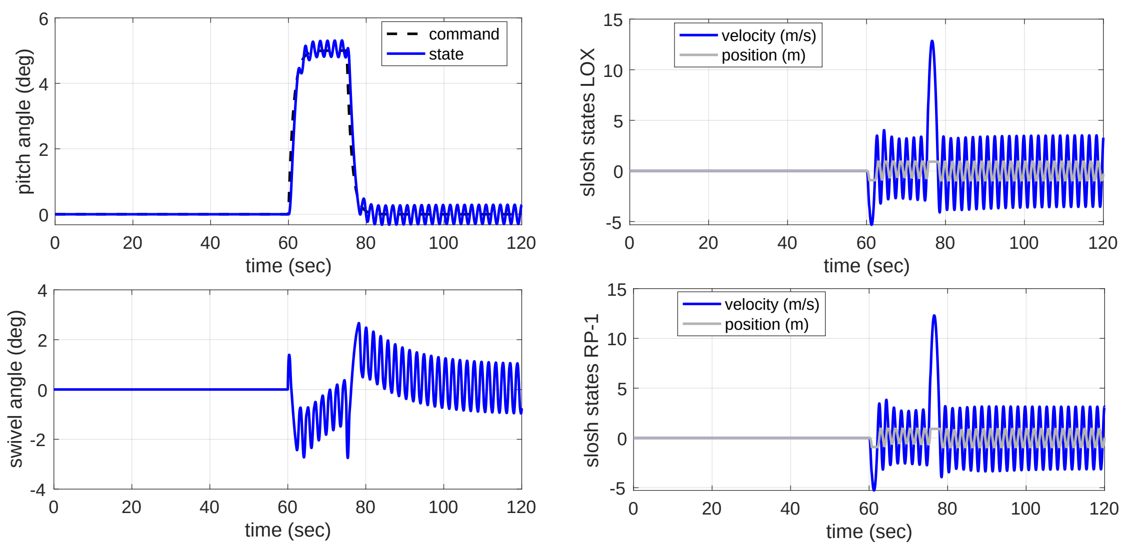

Figure 6. System response after a 2° step in θ; engine dynamics and two flexible modes included (INDI control).

From the earlier research it appeared that in spite of the decent performance for the nominal case, the LQR had a problem to control the plant when besides the slosh motion, the perturbing effect of the flexible modes and the engine dynamics were added. The marginal phase shifts in the feedback signals were already sufficient to destabilise the controller. A preliminary analysis to use a more robust (and non-linear) controller, the INDI, gave promising results.[13] With only the feedback of the rigid-body states θ and q, but otherwise including all effects, the response shown in Fig. 6 was obtained. The coupling with the slosh motion is obvious, and is, of course, not a desired closed-loop response, but realising that this performance is obtained without any slosh knowledge, motivates to adapt such a controller.

As we have discussed earlier, the objective of the current research is to do just that: extend the INDI controller with slosh feedback, and study its performance. In the earlier sections, we have developed controllers based on Incremental Sliding Mode Control (INDI-SMC), and Feedback Linearisation-based Sliding Mode Control (FL-SMC). These controllers will first be evaluated on the nominal plant configuration. For fair comparisons, the sliding surface and SMC parameters used by INDI-SMC and FL-SMC are kept the same, while the differences remain in the linearisation loop (Sec. III.C). The sliding surface parameters in

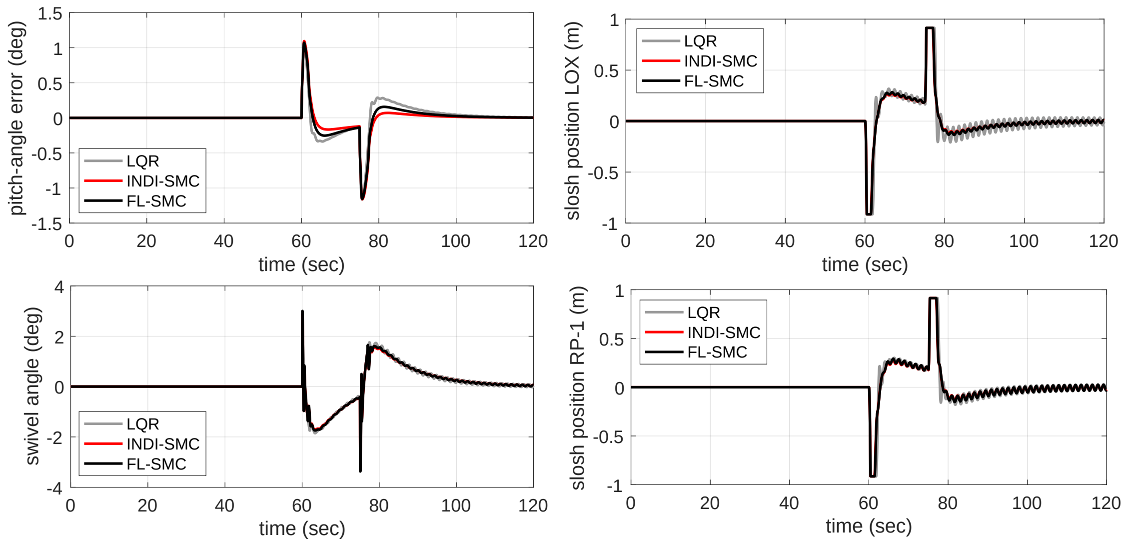

Figure 7. Step response with nominal slosh parameters; $\theta_c = 5°$.

Eq. (20) are selected as $c_\theta = 8$, $c_1 = -0.06$, $c_2 = -0.03$. These parameters are chosen such that $\mathbf{A}_{rr}$ in Eq. (29) is Hurwitz (Theorem 2). The virtual control gains in Theorem 1 are $k_1 = 5$, $k_2 = 5$, $\rho = 0.8$. As discussed in Sec. III.B, the ultimate bound of s can be diminished by amplifying k_2 and reducing ρ. Besides, the convergence rate can be increased by amplifying k_1 (Eq. (24)).

Figure 7 shows the response, including that of the benchmark LQR controller. It is clear that the INDI-SMC and FL-SMC outperform the LQR, which is most obvious from the slosh motion. The LOX slosh-mass position does not show any oscillation anymore, and also the RP-1 slosh mass motion has reduced a bit. In terms of pitch-angle error, both non-linear controllers exhibit smaller errors, with the INDI-SMC being the better one. Note that the slosh-mass positions have been constrained to the tank radius, being $r_{\text{tank}} = 0.9144$ m.

To anticipate on the later sensitivity analysis, in Table 1 the performance indices for these nominal performance simulations have been listed. In Appendix A these indices have been defined; they are related to the integrated state deviation, $\sum_{\theta_{err}}$, the integrated control effort, $\sum_{\varepsilon_T}$, the integrated velocity and position $\sum_{w_s}$ and $\sum_{z_s}$ of the slosh masses (corresponding to the total kinetic and potential energy involved in the slosh motion), and indices representing the amount of oscillation in the signals, *i.e.*, F_θ, F_{ε_T}, F_{w_s}, and F_{z_s}. For each index it holds that the smaller the value the better the controller performance. So, going over the values in the table, these confirm the earlier observations. For the two non-linear controllers, the indices are quite close together, apart from the smaller value for $\sum_{\theta_{err}}$.

B. Slosh-Parameter Variation

In this section, the robustness of the controllers is addressed, in case the actual slosh parameters are different from the nominal ones that were used to design the controllers. For all simulations, we perturb the slosh parameters $m_{s,1}$, $\ell_{s,1}$, $\omega_{s,1}$, $\zeta_{s,1}$, $m_{s,2}$, $\ell_{s,2}$, $\omega_{s,2}$, and $\zeta_{s,2}$, where ω_s and ζ_s have been selected as an alternative to k_s and c_s, respectively. These changes reflect as changes in the plant model, *i.e.*, the state and control matrices $\mathbf{A}'$ and $\mathbf{B}'$ in Eq. (2). The controller gains that were obtained during the design process for the nominal plant are kept constant. For all Monte-Carlo batches, we execute 500 simulations, with perturbed slosh parameters drawn from a uniform distribution. The random generator is reinitialised to its default settings after each batch.

To begin with, and to have a basis for comparison, in Fig. 8(a) the results are shown using the LQR. A 5% variation of the slosh parameters is applied, and the manoeuvre is a two-degree step command on the pitch angle. Even though it might seem that pitch control is not that bad, if one studies the integrated control effort it becomes clear that there are many outliers requiring a significant control effort. For the

Table 1. Performance indices of nominal simulation; $\theta_c = 5°$.

parameter	unit	LQR	INDI-SMC	FL-SMC
$\sum_{\theta_{err}}$	°s	3.7	2.6	3.1
$\sum_{\varepsilon_T}$	°s	15.6	15.4	15.5
$\sum_{w_{s,RP-1}}$	m	5.5	2.9	2.9
$\sum_{z_{s,RP-1}}$	m s	3.5	3.2	3.2
$\sum_{w_{s,LOX}}$	m	4.9	3.6	3.6
$\sum_{z_{s,LOX}}$	m s	3.4	3.2	3.2
F_θ	°	0.5	0.5	0.5
F_{ε_T}	°	2.0	3.5	3.6
$F_{w_{s,RP-1}}$	m/s	4.5	4.2	4.2
$F_{z_{s,RP-1}}$	m	1.0	0.7	0.7
$F_{w_{s,LOX}}$	m/s	4.7	4.3	4.3
$F_{z_{s,LOX}}$	m	1.1	0.7	0.7

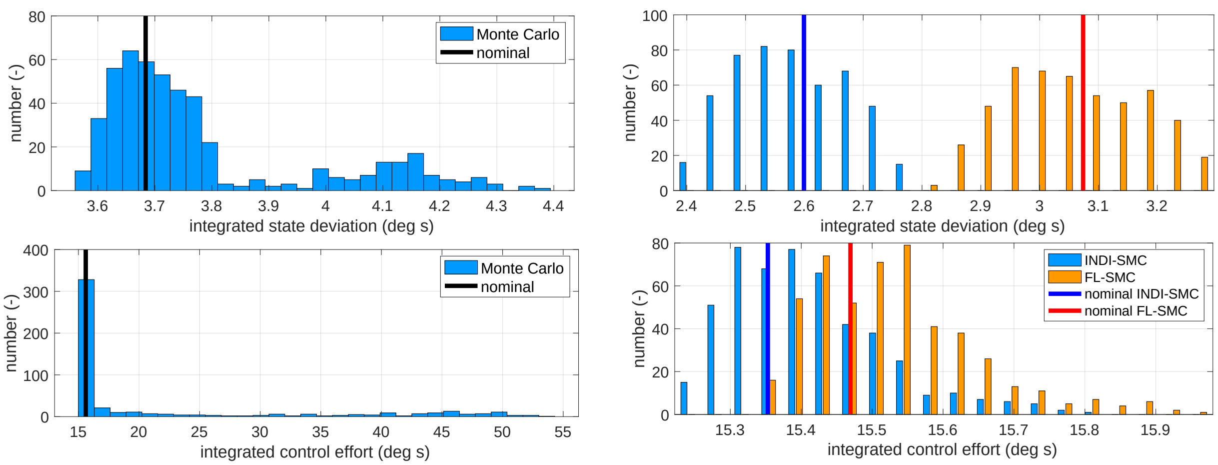

(a) LQR

(b) INDI-SMC and FL-SMC

Figure 8. Monte-Carlo results for 5% slosh-parameter variation; $\theta_c = 2°$.

sake of comparison, in Table 2 the mean value, μ, standard deviation, σ, and the maximum outlier (max) for this analysis have been listed, as well as the corresponding values for the other two controllers. It is evident that the two new controllers are much more robust under the slosh-parameter variations. As visual support, in Fig. 8(b) the integrated state deviation and integrated control effort have been plotted for the same manoeuvre and slosh-parameter variations. The total range for these indices is quite small, as if the controllers are not really affected by the uncertainties. Another observation is that not only is the (nominal) performance of the INDI-SMC better than that of the FL-SMC, it also seems to be more robust, as it experiences fewer outliers.

When we have a closer look at the values in the table, it does show that in terms of robustness, all other performance metrics basically have the same standard deviations, and the maximum values for the outlier are only a bit larger for the FL-SMC. That means that performance-wise the FL-SMC is not that much worse compared to the INDI-SMC. The LQR, on the other hand, shows very large values for some of the standard deviations, and that on top of large mean values. All slosh-related parameters exhibit this behaviour, which confirms that the LQR is not very well capable to suppress the slosh motion in the presence of uncertainties. It could be that the performance of the LQR can be improved, but since it is not the objective of this

Table 2. **Performance indices of Monte-Carlo simulation (5% slosh-parameter variation); $\theta_c = 5°$.**

parameter	unit	LQR			INDI-SMC			FL-SMC		
		μ	σ	max	μ	σ	max	μ	σ	max
$\sum_{\theta_{err}}$	°s	3.8	0.2	4.4	2.6	0.1	2.8	3.1	0.1	3.3
$\sum_{\varepsilon_T}$	°s	21.8	11.1	54.3	15.4	0.1	15.8	15.5	0.1	16.0
$\sum_{w_{s,RP-1}}$	m	28.4	38.3	131.0	4.5	1.6	9.0	4.5	1.6	8.8
$\sum_{z_{s,RP-1}}$	m s	8.1	8.0	29.6	3.3	0.3	4.2	3.4	0.3	4.3
$\sum_{w_{s,LOX}}$	m	23.2	31.8	117.1	6.7	3.2	14.5	6.7	3.2	14.6
$\sum_{z_{s,LOX}}$	m s	7.1	6.7	26.9	3.6	0.5	4.8	3.7	0.5	4.9
F_θ	°	0.6	0.0	0.7	0.5	0.0	0.5	0.5	0.0	0.5
F_{ε_T}	°	3.5	3.0	13.7	3.6	0.1	3.8	3.6	0.1	3.8
$F_{w_{s,RP-1}}$	m/s	9.2	8.4	36.1	4.4	0.2	4.8	4.3	0.1	4.8
$F_{z_{s,RP-1}}$	m	2.1	1.8	8.0	0.8	0.0	0.9	0.8	0.0	0.9
$F_{w_{s,LOX}}$	m/s	8.2	6.7	31.6	4.7	0.4	6.2	4.7	0.4	6.1
$F_{z_{s,LOX}}$	m	1.8	1.5	7.1	0.8	0.1	1.2	0.8	0.1	1.2

research, we will not use the LQR any further – also, because the range of uncertainties could not be further increased with stable responses. Instead, we will do the final analyses with the two non-linear controllers.

The final two batches concerned a 5°-step command on the pitch angle (rather than $\theta_c = 2°$), to explore a bit more of the transient effects, in combination with both 5% and 10% variation of the slosh parameters. As the interpretation of the results in both cases is similar, we will only present the 10%-uncertainty case. The results of this batch are shown in Figs. 9 and 10. From both figures, it is clear that both controllers are very well capable of executing the commands, while maintaining stability. The INDI-SMC has a better nominal performance, shows more results left of this, and has smaller values for the maximum outliers than the FL-SMC. Contrary, the FL-SMC has some smaller minimum outliers. Figure 9(b) shows that the oscillatory behaviour in the pitch and swivel angle is smaller for the INDI-SMC, albeit marginally smaller for θ. However, for ε_T, the difference is more pronounced. Also, Fig. 10 confirms that there is less energy involved in the slosh motion, when controlled with INDI-SMC, and fewer oscillations.

Even though comparable in performance, the overall conclusion seems to be that of the two studied controllers the INDI-SMC is the better one. This will, of course, have to be verified by introducing more non-linearities in the model. In the next and final section, we will include the flexible-body and engine dynamics, and study how the system behaves.

C. Aeroelasticity and Engine Dynamics

In this last section, we will study the controller robustness after adding unmodelled dynamics, *i.e.,* two flexible modes of the launcher structure. We kick off with a nominal simulation, *i.e.,* nominal slosh parameters and a step response of $\theta_c = 5°$. In Figs. 11 and 12, the results for the INDI-SMC are shown – those obtained with the FL-SMC are quite similar. A marginal effect of the rigid-flexible-body coupling can be seen, but this is more obvious in the flexible-body coordinates that clearly show a coupling with the slosh states. The slosh motion induces a small structural vibration, which, for the structural design, should be analysed in more detail in case this can potentially cause damage. All in all, the controller(s) does not seem to be affected much by these additional dynamics. For reference, in Table 3 the corresponding performance indices are listed, for both controllers. These can serve as a baseline for interpreting the results of the upcoming Monte-Carlo analysis.

There are some differences, most notably in $\sum_{\theta_{err}}$ and the slosh-related parameters, in favour of the INDI-SMC having the smaller values. We have added the integrated effects of the generalised flexible-body velocity and position, as well as the corresponding oscillation indices. The former two may be interpreted as an indicators for the elastic kinetic and potential energy, whereas, for instance, F_{η_1} can serve as indicator for

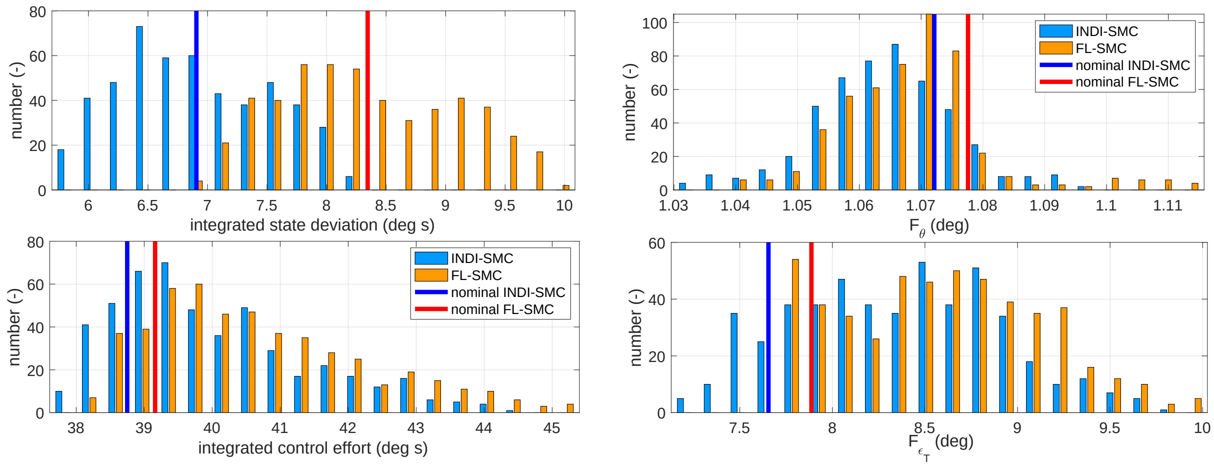

(a) state deviation and control effort

(b) state and control oscillations

Figure 9. Monte-Carlo results for 10% slosh-parameter variation; $\theta_c = 5°$.

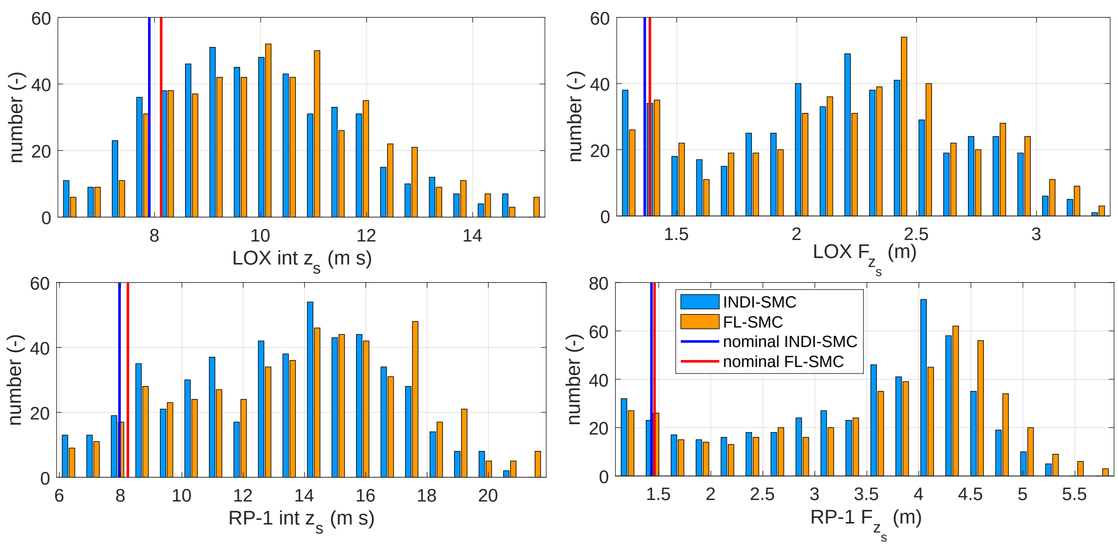

Figure 10. Monte-Carlo results for 10% slosh-parameter variation, $\theta_c = 5°$: slosh parameters.

the amount of vibration. For the nominal case, the excitation of the modes is the same for both controllers. As was to be expected, judging from the eigenfrequencies of the two modes, *i.e.,* 37.3 and 105 rad/s, respectively,[13] the first bending mode is dominating and will be the one to be studied below.

The final analysis we will do is a 10% variation of the slosh parameters. Again, 500 simulations per batch are executed, and the variations are drawn from a uniform distribution. For either controller, the random generator is initialised with the same seed. The results are shown in Figs. 14 through 15, supported by the data in Table 4. In all aspects, the INDI-SMC performs better than the FL-SMC. For the integrated state deviation, the tendency is that more simulations end up with a smaller value than the nominal one, whereas for the FL-SMC this is less pronounced. Concerning the integrated control effort, the distribution for the FL-SMC is more skewed with some more outliers towards the maximum. The oscillations in θ are marginal, and both controllers can suppress this well. The oscillations in the swivel angle is a little more noticeable, but this does not seem to be a problem.

The variation in the slosh parameters leads to a stronger coupling with the flexible modes, as shown in Fig. 14. The INDI-SMC suppresses the vibrations a bit better, but this is a consequence of more stable control of the slosh modes. The differences are not very large, but present nonetheless.

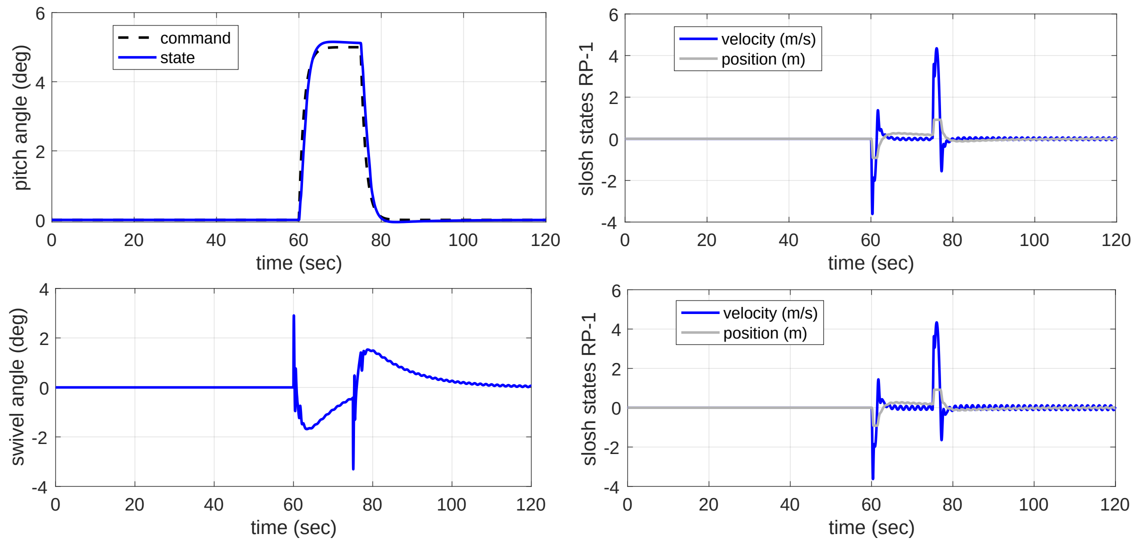

Figure 11. Step response with nominal slosh parameters ($\theta_c = 5°$). Launcher with flexible dynamics, INDI-SMC controller.

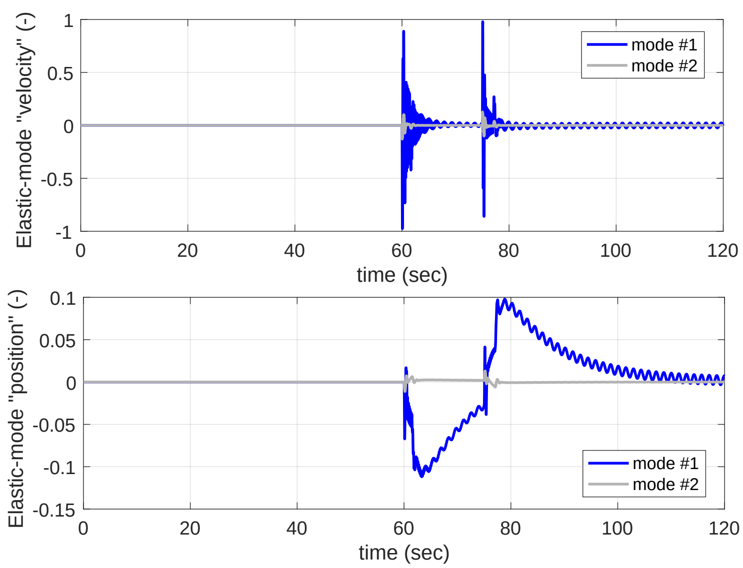

Figure 12. Flexible modes after a step response with nominal slosh parameters ($\theta_c = 5°$). Launcher with flexible dynamics, INDI-SMC controller.

Comparing the results with the corresponding plots, Figs. 9 and 10 shows that the addition of the unmodeled flexible dynamics does not degrade the controller performance too much. Both controllers do an excellent job, but the winner in this case is the INDI-SMC.

The final test of robustness is to simulate a 5°-step response for the complete system, *i.e.,* the flexible launcher with engine dynamics and sloshing in the fuel and oxidiser tanks. Initial runs indicated a high-frequency oscillatory motion of the swivel command, which could not be resolved by tuning the controller. However, the origin of the oscillations was traced back to the actuator feedback loop, which amplified the oscillations in the system. Therefore, we included a first-order low-pass filter (with a bandwidth equal to 30 rad/s) in this feedback loop, which solved the problem. The final results are shown in Figs. 16 and 17. From these results, the robust performance of the INDI-SMC controller is obvious, but it is also clear that attention should be paid to the actuator-feedback loop. It does not suffice to just use the previous command value issued by the controller.

Table 3. Performance indices of nominal simulation with flexible dynamics; $\theta_c = 5°$.

parameter	unit	INDI-SMC	FL-SMC
$\sum_{\theta_{err}}$	°s	6.9	8.3
$\sum_{\varepsilon_T}$	°s	38.3	38.7
$\sum_{\dot{\eta}_1}$	s	1.7	1.9
$\sum_{\eta_1}$	s	2.2	2.2
$\sum_{\dot{\eta}_2}$	s	0.1	0.1
$\sum_{\eta_2}$	s	0.1	0.1
$\sum_{w_{s,RP-1}}$	m	12.3	13.4
$\sum_{z_{s,RP-1}}$	m s	7.9	8.1
$\sum_{w_{s,LOX}}$	m	13.9	15.4
$\sum_{z_{s,LOX}}$	m s	8.0	8.3
F_θ	°	1.1	1.1
F_{ε_T}	°	7.7	7.9
$F_{\dot{\eta}_1}$	-	2.9	3.2
F_{η_1}	-	0.2	0.2
$F_{\dot{\eta}_2}$	-	0.4	0.4
F_{η_2}	-	0.0	0.0
$F_{w_{s,RP-1}}$	m/s	7.6	7.8
$F_{z_{s,RP-1}}$	m	1.4	1.4
$F_{w_{s,LOX}}$	m/s	7.9	8.2
$F_{z_{s,LOX}}$	m	1.4	1.5

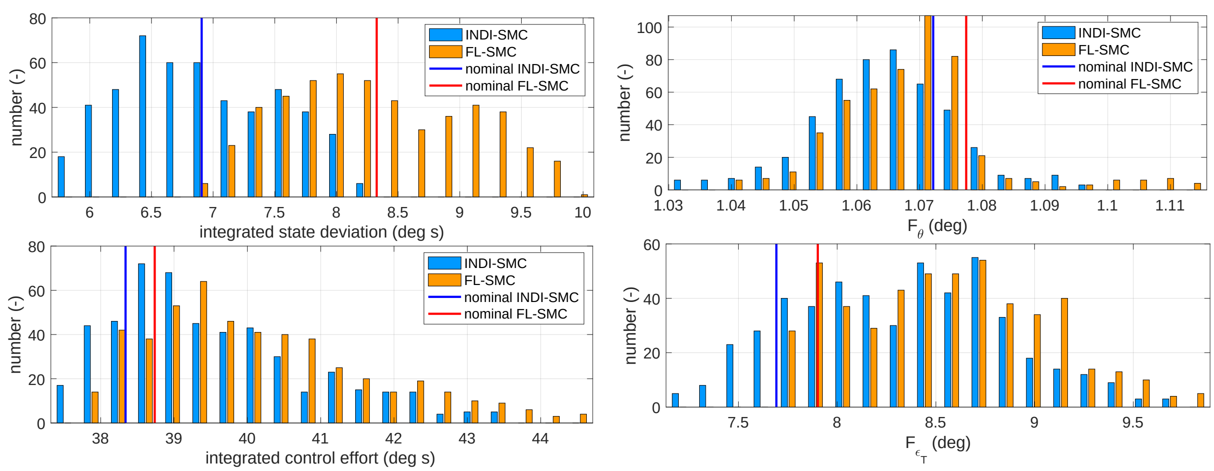

(a) state deviation and control effort

(b) state and control oscillations

Figure 13. Monte-Carlo results for 10% slosh-parameter variation ($\theta_c = 5°$); launcher with flexible dynamics.

V. Conclusions and Recommendations

This paper focuses on the attitude control and slosh dynamic suppression of an aeroelastic launch vehicle with non-linear engine dynamics. A series of damped mass-spring systems are used to model the slosh dynamics in the fuel and oxidiser tanks of the PacAstro launch vehicle. The resulting slosh dynamics is

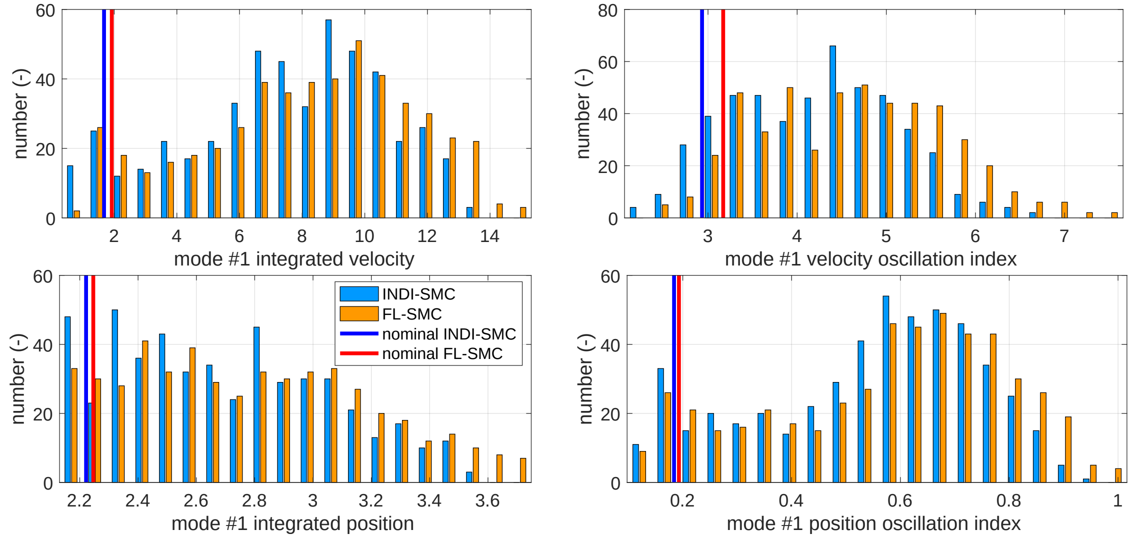

Figure 14. Monte-Carlo results for 10% slosh-parameter variation ($\theta_c = 5°$): slosh parameters. Launcher with flexible dynamics.

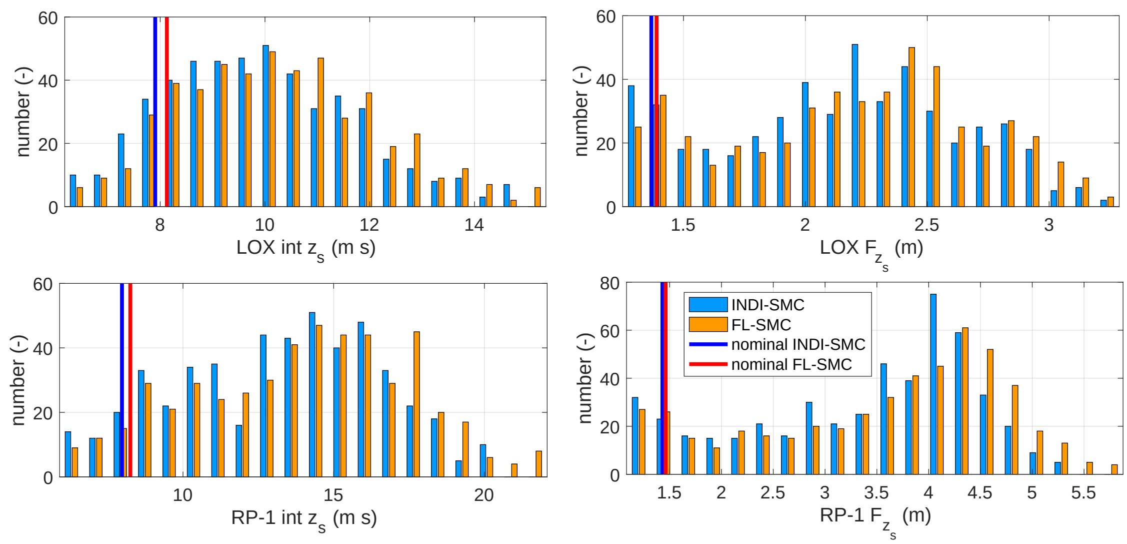

Figure 15. Monte-Carlo results for 10% slosh-parameter variation ($\theta_c = 5°$): slosh parameters. Launcher with flexible dynamics.

tightly coupled with the rigid-body dynamics, which, if not properly dealt with, can destabilise the entire launch vehicle.

In literature, the Linear-quadratic Regulator (LQR) has been applied to this problem. Although the vehicle under LQR control can track the pitch angle command, limit-cycle behaviour presents itself in the swivel commands. Moreover, the performance of LQR degrades in the presence of model uncertainties and unmodeled dynamics (aeroelastic modes, engine dynamics, *etc.*). In view of these limitations, the Incremental Non-linear Dynamic Inversion (INDI) control was proposed for launch-vehicle control. It has been shown that INDI indeed has superior performance in terms of state deviation and control effort. However, since conventional INDI control cannot handle under-actuated systems, the slosh dynamics cannot be effectively suppressed. As a consequence, limit-cycle behaviour still presents itself under INDI control.

This paper adopts the novel Incremental Sliding Mode Control (INDI-SMC) to deal with the under-actuated dynamics and to enhance the robustness of INDI control further. Apart from the inherent robustness of Sliding Mode Control (SMC) to the so-called matched uncertainties, the sliding surface designed in

Table 4. **Performance indices of Monte-Carlo simulation with flexible dynamics (10% slosh-parameter variation); $\theta_c = 5°$.**

parameter	unit	INDI-SMC			FL-SMC		
		μ	σ	max	μ	σ	max
$\sum_{\theta_{err}}$	°s	7.0	0.6	8.4	8.4	0.7	10.0
$\sum_{\varepsilon_T}$	°s	39.7	1.3	43.8	40.3	1.5	44.8
$\sum_{\dot\eta_1}$	s	7.8	3.2	14.0	8.5	3.4	15.6
$\sum_{\eta_1}$	s	2.7	0.4	3.6	2.8	0.4	3.8
$\sum_{\dot\eta_2}$	s	0.2	0.1	0.4	0.2	0.1	0.4
$\sum_{\eta_2}$	s	0.1	0.0	0.1	0.1	0.0	0.1
$\sum_{w_{s,RP-1}}$	m	30.6	10.9	56.4	32.3	11.3	59.2
$\sum_{z_{s,RP-1}}$	m s	10.1	1.8	15.0	10.5	1.9	15.5
$\sum_{w_{s,LOX}}$	m	49.8	18.1	82.2	53.4	19.3	90.8
$\sum_{z_{s,LOX}}$	m s	13.6	3.4	20.8	14.3	3.6	22.3
F_θ	°	1.1	0.0	1.1	1.1	0.0	1.1
F_{ε_T}	°	8.4	0.5	9.7	8.6	0.5	10.0
$F_{\dot\eta_1}$	-	4.3	0.9	6.9	4.8	1.0	7.8
F_{η_1}	-	0.6	0.2	1.0	0.6	0.2	1.0
$F_{\dot\eta_2}$	-	0.4	0.0	0.5	0.4	0.0	0.5
F_{η_2}	-	0.0	0.0	0.0	0.0	0.0	0.0
$F_{w_{s,RP-1}}$	m/s	10.7	1.9	14.6	11.1	2.0	15.1
$F_{z_{s,RP-1}}$	m	2.2	0.5	3.3	2.3	0.5	3.3
$F_{w_{s,LOX}}$	m/s	16.2	4.5	24.2	17.1	4.9	25.6
$F_{z_{s,LOX}}$	m	3.5	1.1	5.4	3.7	1.2	5.9

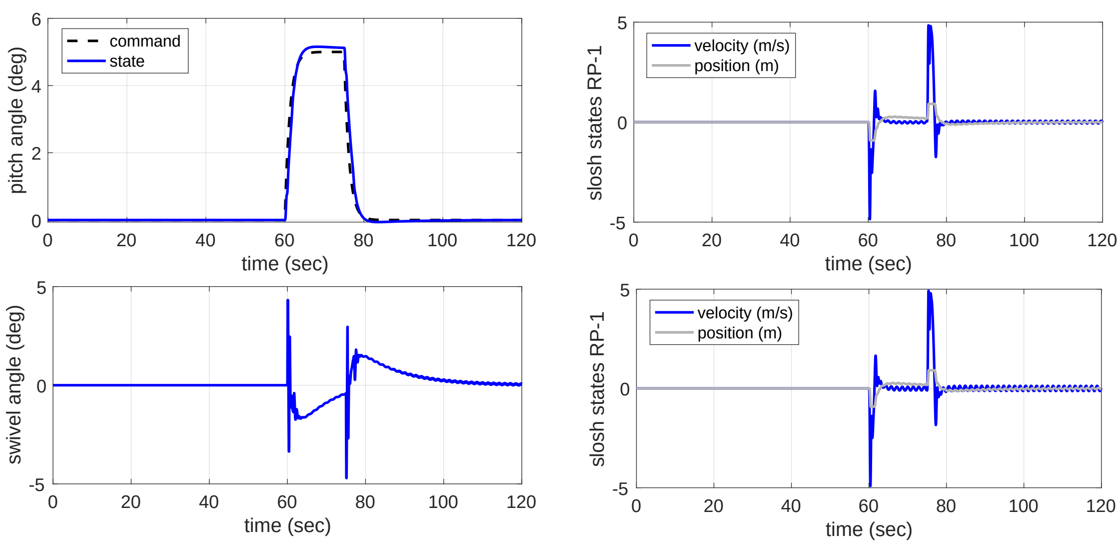

Figure 16. **Step response ($\theta_c = 5°$) of flexible launcher, with sloshing and engine dynamics (INDI-SMC).**

this paper also ensures the robustness against unmatched uncertainties. The stability of the proposed controller is proved using Lyapunov methods. Different from the conventional SMC designs based on Feedback

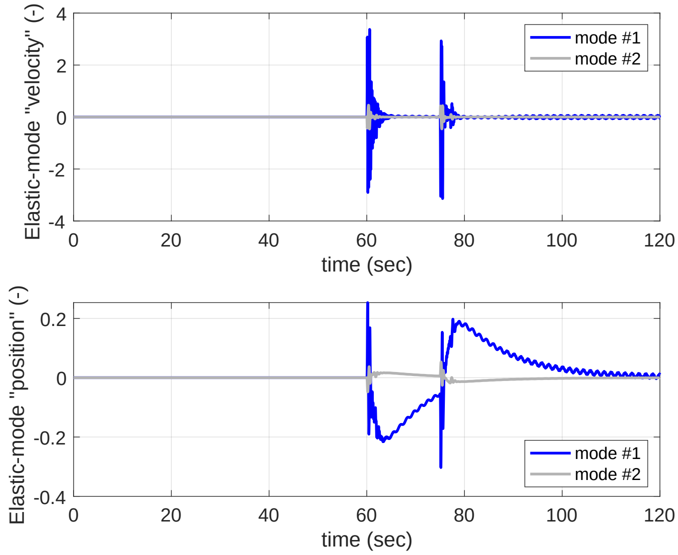

Figure 17. Step response ($\theta_c = 5°$) of flexible launcher, with sloshing and engine dynamics: flexible modes (INDI-SMC).

Linearisation (FL), the only model information needed by INDI-SMC is the control effectiveness. Even so, by excavating the sensor measurements, INDI-SMC still has better robustness against model uncertainties and external disturbances than its FL-SMC counterpart.

The merits of INDI-SMC over LQR, INDI, and FL-SMC are verified by numerical simulations. In the nominal case, conventional INDI control (without slosh-state feedback) is unable to suppress the slosh dynamics. On the contrary, all the other three controllers can enhance the slosh damping. A sensitivity analysis also shows that INDI-SMC and FL-SMC can more effectively damp out the slosh motions than the LQR. Moreover, the pitch-angle tracking error under the control of INDI-SMC is the smallest.

Monte-Carlo studies have been used to evaluate the robustness of the controllers to parametric uncertainties. When a 5% variation of the slosh parameters and a 2°-step command on the pitch angle is applied, the system using LQR has many outliers requiring significant control efforts. Also, the performance metrics for LQR present both the highest mean values and the largest standard deviations among all the tested controllers. To further distinguish the difference between INDI-SMC and FL-SMC, the parameter variation range and the step command magnitude are amplified to 10% and 5°, respectively. Under this circumstance, both INDI-SMC and FL-SMC can execute the command, while damping the slosh motions. However, INDI-SMC has better nominal performance, as well as smaller values for the maximum outliers than FL-SMC. The slosh energy using INDI-SMC is lower as well. It is worth noting that INDI-SMC also requires less model information than FL-SMC.

The robustness of the controller to unmodeled dynamics has also been evaluated. Adding two flexible modes of the structural model to the plant shows that either controller can handle this well, even in the presence of 10% variation in the slosh parameters. Coupling between the slosh and flexible modes is observed, which may be studied in more detail once a more advanced structural model of the launcher is available. After the inclusion of a third-order engine dynamics, the actuator feedback loop had oscillations. Inserting a low-pass filter in this loop solved this issue, and a very robust control response was obtained. It is stressed, though, that attention should be paid to the actuator-feedback loop. It does not suffice to just use the previous command value issued by the controller, because it does not always reflect the hardware state.

For all performance indices studied, the INDI-SMC is the more robust controller. Most notable differences are found in the integrated state deviation and the slosh motion, but this also reflects as a smaller excitation of the flexible modes.

For future work, it is recommended to design a robust observer for both the rigid-body and the slosh states. Modelling the slosh dynamics as (non-linear) damped pendulum systems and comparing the resulting model properties with the damped mass-spring systems is also recommended. The ultimate goal of this research is to design non-linear and robust controllers and observers for fully non-linear launch-vehicle dynamics.

References

[1]Lester, H.C. and Collins, D.F., "Determination of Launch-Vehicle Response to Detailed Wind Profiles", AIAA-64-82, *Aerospace Sciences Meeting*, New York, NY, 1964.

[2]Meirovitch, L., and Wesley, D. A., "On the Dynamic Characteristics of a Variable-Mass Slender Elastic Body Under High Accelerations", *AIAA Journal*, Vol. 5, No. 8, 1967, pp. 1439-1447.

[3]Geissler, E.D., "Wind Effects on Launch Vehicles", AGARDograph No. 115, 1970.

[4]Orr, J.S., "A Coupled Aeroelastic Model for Launch Vehicle Stability Analysis", AIAA-2010-7642, *AIAA Atmospheric Flight Mechanics Conference*, Toronto, Canada, 2-5 August 2010.

[5]Mooij, E. and Gransden, D. I., "The Impact of Aeroelastic Effects on the controllability of Conventional Launch Vehicles", *Proceedings of the 67th IAC Conference*, Guadalajara, Mexico, September, 2016.

[6]Mooij, E. and Gransden, D. I., "Quasi-Transient Stability Analysis of a Conventional Aeroelastic Launch Vehicle", *Proceedings of the 68th IAC Conference*, Adelaide, Australia, September 25-29, 2017.

[7]Cui, D.-L., Yan, S.-Z., Guo, X.-S. and Gao, R.X., "Parametric Resonance of Liquid Sloshing in Partially Filled Spacecraft Tanks During the Powered-Flight Phase of Rocket", *Aerospace Science and Technology*, Vol. 35, May 2014, pp. 93–105.

[8]Ottander, J.A., Hally, R.A. and Powers, J.F., "Practical Methodology for the Inclusion of Non-linear Slosh Damping in the Stability Analysis of Liquid-propelled Space Vehicles", AIAA-2018-2097, *AIAA SciTech Forum, Guidance, Navigation, and Control Conference*, Kissimmee, Florida, 8-12 January 2018.

[9]Shekhawat, A., Nichkawde, C. and Ananthkrishnan, N., "Modeling and Stability Analysis of Coupled Slosh-Vehicle Dynamics in Planar Atmospheric Flight", AIAA-2006-0427, *44th AIAA Aerospace Sciences Meeting and Exhibit*, Reno, NV, 9-12 January, 2006.

[10]Reyhanoglu, M. and Rubio Hervas, J., "Non-linear Dynamics and Control of Space Vehicles with Multiple Fuel Slosh Modes", *Control Engineering Practice*, Vol. 20, 2012, pp. 912–918.

[11]Rubio Hervas, J. and Reyhanoglu, M., "Thrust-Vector Control of a Three-Axis Stabilized Upper-Stage Rocket with Fuel Slosh Dynamics", *Acta Astronautica*, Vol. 98, 2014, pp. 120–127.

[12]Mooij, E. and Gransden, D.I., "The Effect of Sloshing on the Controllability of a Conventional Aeroelastic Launch Vehicle", AIAA-2019-0116, *AIAA SciTech Forum, Guidance, Navigation, and Control Conference*, San Diego, CA, 5-9 January 2019.

[13]Mooij, E., "Slosh Observer Design for Aeroelastic Launch Vehicles", AIAA-2020-1606, *AIAA SciTech Forum, Guidance, Navigation, and Control Conference*, Orlando, Florida, 6-10 January 2020.

[14]Fleeter, R., Mcloughlin, F. and Mills, R., "A Low-Cost Expendable Launch Vehicle for 500-Pound Class Satellites", Marketing brochure, PacAstro, Herndon, VA, 26 May 1992.

[15]Abramson, H.N., "The dynamic behavior of liquids in moving containers: with applications to space vehicle technology", NASA SP-106, 1966.

[16]Abramson, H.N., Chapter 8, "Liquid Propellant Dynamics", in: Mazet, R., *Manual on Aeroelasticity*, Volume I, AGARD Report R-578, 1968.

[17]Dodge, F., "The New "Dynamic Behavior of Liquids in Moving Containers", Southwest Research Inst., 2000.

[18]Stephens, D., Leonard, H.W. and Perry, T.W., "Investigation of the Damping of Liquids in Right-Circular Cylindrical Tanks, Including the Effects of a Time-Variant Liquid Depth", NASA-TN-D-1367, 1962.

[19]Wang, X., van Kampen, E., Chu, Q., and Lu, P., "Incremental Sliding-Mode Fault-Tolerant Flight Control", *Journal of Guidance, Control, and Dynamics*, Vol. 42, no. 2, pp. 244–259, Feb 2019.

[20]Wang, X., Sun, S., van Kampen, E., and Chu, Q., "Quadrotor Fault Tolerant Incremental Sliding Mode Control driven by Sliding Mode Disturbance Observers", *Aerospace Science and Technology*, Vol. 87, pp. 417-430, 2019.

[21]Wang, X., van Kampen, E., and Chu, Q., "Comparison of three control structures for inducing higher-order sliding modes", *18th European Control Conference (ECC)*, pp. 4073-4080, 2019.

[22]Khalil, H.K., *Non-linear Systems*, Prentice-Hall, New Jersey, 2002.

[23]Yu, S., Yu, X., Shirinzadeh, B., and Man, Z., "Continuous finite-time control for robotic manipulators with terminal sliding mode", *Automatica*, Vol. 41, No. 11, 2005, pp. 1957–1964.

[24]Sieberling, S., Chu, Q., and Mulder, J. A., "Robust Flight Control Using Incremental Non-linear Dynamic Inversion and Angular Acceleration Prediction", Journal of Guidance, Control, and Dynamics, Vol. 33, No. 6, 2010, pp. 1732–1742.

[25]Wang, X., van Kampen, E., Chu, Q., and Lu, P., "Stability Analysis for Incremental Non-linear Dynamic Inversion Control", Journal of Guidance, Control, and Dynamics, Vol. 42, No. 5, 2019, pp. 1116–1129.

[26]Grondman, F., Looye, G., Kuchar, R. O., Chu, Q., and van Kampen, E., "Design and Flight Testing of Incremental Non-linear Dynamic Inversion-based Control Laws for a Passenger Aircraft", 2018 AIAA Guidance, Navigation, and Control Conference, Kissimmee, Florida, 2018.

Appendix A. Controller Performance Indices

To compare the controller responses and the effect of sloshing, several performance metrics will be defined. The first one is the minimum attitude deviation of the launcher with respect to the guidance commands, whereas the second one is the swivel effort that is required to achieve this. These two objectives can be expressed as the integrated pitch-angle deviation and the integrated swivel angle (equivalent to, for instance, the total hydraulic power required), given by:

$$\sum_{\theta_{err}} = \int_0^{\mathrm{T}} |\theta_c(t) - \theta_p(t)| \mathrm{d}t \qquad \sum_{\varepsilon_T} = \int_0^{\mathrm{T}} |\varepsilon_T(t)| \mathrm{d}t \tag{32}$$

A graphic representation of the above metrics is shown in Fig. A1(a), represented by the grey areas, for a 2° step command in θ, starting at $\Delta t = 1$ s with a duration of 14 s. For optimal controller performance, both individual areas should be as small as possible, which means that their numerical equivalent can be used to evaluate different controller designs. In the given example, $\sum_{\theta_{err}} = 6.55°$s and $\sum_{\varepsilon_T} = 17.21°$s.

Another metric can be the oscillatory behaviour of either state or control variable. Oscillations in the control may not only be energy expensive and a burden on the hardware, it could also lead to instabilities. Equivalently, oscillations in the slosh states gives an indication of the severity of the motion and potential hazardous situations. To detect oscillations or otherwise discrete changes in the controls, the cumulative moving standard deviation can be used. For a subset j of n_s out of a total of N samples of an arbitrary control signal u, the moving mean is defined as $\bar{y}_j = \frac{1}{n_s} \sum_{i=j}^{j+n_s-1} u_i$. Here, j will run from $j = 1{+}n_s/2$ to N-$n_s/2$, so each subsequent subset will shift by only one sample. Let the squared deviation from this mean be defined as $s_{u,j} = (u_{j+n_s/2} - \bar{y}_j)^2$, which represents the value at the midpoint of subset j. The cumulative standard deviation, F_u, for subset j is then

$$F_{u_j} = \sqrt{\frac{1}{N - n_s - 1} \sum_{k=1}^{j} s_k} \tag{33}$$

As an example, in Fig. A1(b) the oscillation pattern of the slosh velocity is shown, due to a poorly designed control system. The cumulative standard deviation increases more rapidly when a discrete jump occurs, or when there is an interval with persistent oscillations. As a metric, the grey area under the curve can be used, which, while minimised, would lead to a smoother behaviour. In this particular example, the numerical value is $F_{z_s} = 35.6$ m/s.

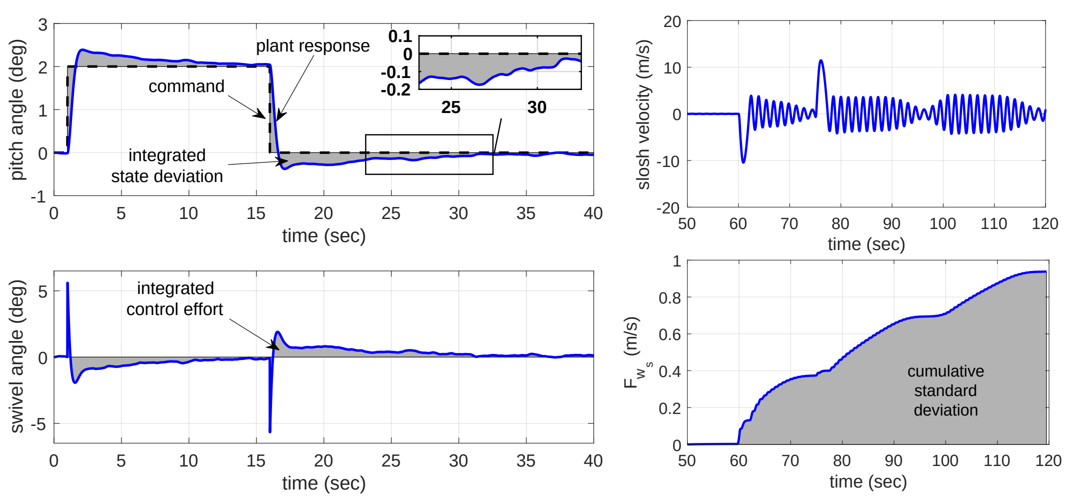

(a) State deviation and control effort (b) Oscillatory behaviour

Figure A1. Controller performance indices.